


RESEARCH

Open Access



Establishment of a prognostic model based on ER stress-related cell death genes and proposing a novel combination therapy in acute myeloid leukemia

Minghui Wang^{1†}, Huajian Xian^{1†}, Xiaoli Xia¹, Wenjie Zhang¹, Zixuan Huang^{1,2}, Chaoqun Lu¹, Yuling Zheng¹, Yixin Wang¹, Shufeng Xie^{1,2}, Renyao Pan¹, YaoYifu Yu^{1,2}, Ruiheng Wang^{1,2}, Huijian Zheng¹, Guorui Huang^{3*} and Han Liu^{1,2*} 

Abstract

Background Acute myeloid leukemia (AML) is a highly heterogeneous malignancy, presenting significant challenges in accurately predicting patient prognosis. Dysregulation of endoplasmic reticulum (ER) stress and resistance to programmed cell death (PCD) are hallmarks of AML cells. However, the prognostic significance of the interplay between ER stress and cell death pathways in AML remains largely unexplored.

Methods We analyzed RNA sequencing and clinical data from 887 AML patients across 4 cohorts to develop an ER stress-related cell death index (ERCDI) using 10 machine-learning algorithms with 117 unique combinations. Survival and time-dependent Receiver Operating Characteristic Curve (ROC) analyses were performed to assess the model's efficacy. Clinical characteristics, the tumor immune microenvironment, and drug sensitivity differences between the high- and low-risk groups were also analyzed. The CMap database was used to identify potential therapeutic drugs. In vitro and in vivo experiments, including CCK-8, colony formation, flow cytometry, Transwell assays, and xenograft mouse models, were conducted to evaluate the effects of the target genes and candidate drugs.

Results The ERCDI demonstrated strong prognostic and predictive performance for prognosis in AML patients. Furthermore, the ERCDI effectively predicted immunotherapy and chemotherapy outcomes and was associated with the immune features of the different risk groups. DNA damage-inducible transcript 4 protein (DDIT4), a key gene associated with ERCDI, is related to poor prognosis in AML patients with high expression. Additionally, the knockdown of DDIT4 significantly inhibited AML cell proliferation, induced cell apoptosis, and promoted cell cycle arrest. Chaetocin was subsequently identified as a candidate compound for AML treatment. Subsequent experiments suggested that combining chaetocin and venetoclax is a potentially promising therapeutic strategy for AML.

Conclusion The ERCDI provides personalized risk assessment and treatment recommendations for individual AML patients. The combined use of chaetocin and venetoclax can potentially be repurposed for AML therapy.

[†]Minghui Wang and Huajian Xian contributed equally to this work.

*Correspondence:

Guorui Huang
hgr12038@rjh.com.cn
Han Liu
liuhan68@sjtu.edu.cn

Full list of author information is available at the end of the article



© The Author(s) 2025. **Open Access** This article is licensed under a Creative Commons Attribution-NonCommercial-NoDerivatives 4.0 International License, which permits any non-commercial use, sharing, distribution and reproduction in any medium or format, as long as you give appropriate credit to the original author(s) and the source, provide a link to the Creative Commons licence, and indicate if you modified the licensed material. You do not have permission under this licence to share adapted material derived from this article or parts of it. The images or other third party material in this article are included in the article's Creative Commons licence, unless indicated otherwise in a credit line to the material. If material is not included in the article's Creative Commons licence and your intended use is not permitted by statutory regulation or exceeds the permitted use, you will need to obtain permission directly from the copyright holder. To view a copy of this licence, visit <http://creativecommons.org/licenses/by-nc-nd/4.0/>.

Keywords Acute myeloid leukemia, ER stress, Programmed cell death, Machine learning, DDIT4, Chaetocin, Venetoclax, Combination therapy

Introduction

AML is a hematologic malignancy characterized by the abnormal proliferation of hematopoietic stem cells or early progenitors [1–3]. Although current treatments, including chemotherapy, targeted therapy, and hematopoietic stem cell transplantation (HSCT), have improved outcomes, the overall 5-year survival rate for AML patients remains unsatisfactory [4]. Relapse and resistance to therapy remain intractable issues in clinical practice [5–7]. Identifying genes and biological processes involved in the pathogenesis of AML and those contributing to therapeutic resistance is crucial for improving clinical outcomes. Furthermore, advancements in therapy may stem from more precise risk stratification, enabling better management and treatment for AML patients.

Currently, the most commonly applied approach for AML risk stratification is the European LeukemiaNet (ELN), which stratifies patients into different risk groups according to cytogenetic and chromosomal abnormalities [8]. However, this method is often costly and time-consuming. Transcriptome-based prognostic models have gained increasing attention. Among them, the LSC17 score, which was developed based on gene expression profiles of leukemia stem cells (LSCs), is among the most widely recognized, as LSCs are believed to play a pivotal role in AML initiation, progression, and drug resistance [9]. Nevertheless, several studies have suggested that LSCs may not be enriched in all relapsed or drug-resistant AML patients and that leukemia-regenerating cells emerging after chemotherapy exhibit distinct molecular characteristics from those of therapy-naïve LSCs [10, 11]. Single-cell analysis of AML samples emphasized the essential role of the immune system and inflammatory-related signaling, and corresponding prognostic models have also been reported [12, 13]. However, testing certain molecules, such as inflammatory cytokines and chemokines, is difficult because of their low expression. Therefore, it is critical to identify genes with prognostic value in AML and establish accurate models.

In recent years, ER stress dysregulation has emerged as a hallmark of tumor cells [14–16]. Various changes in the tumor microenvironment, such as nutrient deprivation, low oxygen supply, and metabolite accumulation, trigger ER stress, which is characterized by the activation of three branches of the unfolded protein response (UPR) [17, 18]. Changes in UPR responses

can regulate multiple biological processes, including PCD signals, another important regulatory mechanism [16, 19]. For example, persistent activation of ER stress has been reported to initiate apoptosis via the PKR-like endoplasmic reticulum kinase (PERK)–C/EBP homologous protein (CHOP) axis and to modulate autophagy through either the PERK–nuclear factor erythroid 2-related factor 2 (NRF2) or inositol-requiring enzyme 1 alpha (IRE1α)–c-Jun N-terminal kinase (JNK) signaling pathways [20–22]. Persistent ER stress activation may also inhibit ferroptosis by upregulating the expression of chaperones such as Binding-immunoglobulin protein (Bip) [21]. Conversely, several PCD-related proteins such as Bax inhibitor-1 (BI-1), protein tyrosine phosphatase 1B (PTP-1B), and ASK1-interacting protein 1 (AIP1) directly regulate UPR sensor IRE1α, indicating a reciprocal regulatory loop [23]. These findings underscore the complexity of ER stress–PCD interactions, where cellular fate is determined by the strength and duration of stress and context-specific signaling crosstalk.

In the context of AML, the dysregulation of ER stress and PCD pathways is prevalent and complex. Accumulating evidence reported that the activation of ER stress in LSCs, particularly the IRE1α–XBP1 s signaling branch, commonly accompanies leukemogenesis [20, 24, 25]. Another key feature of LSCs is impaired apoptotic signaling, which is typically characterized by the upregulation of B-cell lymphoma 2 (BCL-2) expression [26, 27]. Notably, inhibition of the RNase activity of IRE1α in AML cells has been shown to reduce BCL-2 expression, and high expression of the ER co-chaperone DNAJC10 was recently reported in LSCs, the loss of which increased (BCL-2-associated X protein) BAX expression and decreased BCL2 expression through PERK–eIF2α pathway modulation [27, 28]. Intriguingly, in AML subtypes harboring RUNX1 mutations, both UPR and proapoptotic p53 signaling are decreased in LSCs, yet these cells retain a proliferative advantage [29]. These findings highlight the intricate and context-dependent regulatory network between ER stress responses and apoptotic signaling during AML pathogenesis.

ER stress-related signaling pathways are frequently activated within the bone marrow microenvironment (BMME) of AML, and transmissible ER stress, which helps reconstitute the bone marrow niche of AML, has also been reported [30, 31]. In addition to triggered ER stress, several forms of PCD, such as autophagy, are

also activated [32]. In the FLT3-ITD subtype of AML, autophagy can be activated by the eIF2 α -ATF4 signaling axis, indicating a potential regulatory role of ER stress in autophagy [33]. Furthermore, the activation of ER stress promotes the release of damage-associated molecular patterns (DAMPs), such as calreticulin (CRT), heat shock protein 70 (HSP70) and HSP90, which are closely linked to the induction of another type of nonapoptotic PCD known as immunogenic cell death (ICD), thereby influencing the sensitivity of AML patients to immunotherapy [34, 35]. PCD is now known to encompass a broad range of modalities beyond apoptosis and autophagy, including necroptosis, pyroptosis, parthanatos, netotic cell death, lysosome-dependent cell death, ICD, ferroptosis, cuproptosis, entotic cell death, and alkaliptosis [36, 37]. However, the interactions between ER stress and other forms of PCD remain incompletely understood. Importantly, as a critical regulator of cellular homeostasis, ER stress has the dual capacity to promote either cell survival or death. However, the key molecular determinants that govern this cell fate decision remain elusive, underscoring the need to elucidate the mechanistic links between ER stress and various PCD pathways.

Considering the critical roles of ER stress and PCD in maintaining cellular homeostasis and their close interconnections, we first employed a bioinformatics approach to identify key genes involved in the ER stress and PCD pathways. We developed a novel prognostic model, the ERCDI model, for AML. The predictive performance and reliability of the ERCDI were confirmed through comparisons with established AML prognostic models and internal cohort validation. Furthermore, we preliminarily demonstrated the functional role of DDIT4, a core gene of the ERCDI model, in regulating AML cell growth and proliferation. Additionally, we identified small molecules associated with the ERCDI and evaluated their combination efficacy with clinically used drugs. Finally, we proposed a novel therapeutic strategy combining chaetocin and venetoclax. This combination exhibited promising antileukemic effects both in vitro and in vivo.

Materials and methods

Dataset collection

Clinical information and gene expression profiles of AML patients were downloaded from the Gene Expression Omnibus (GEO) (<https://www.ncbi.nlm.nih.gov/geo/>), Therapeutically Applicable Research to Generate Effective Treatment (TARGET) (<https://www.cancer.gov/ccg/research/genome-sequencing/target>), and The Cancer Genome Atlas (TCGA) (<https://www.cancer.gov/tcga/>). Four published datasets were included in this study: GSE37642-GPL96 (n = 417), GSE12417-GPL96 (n = 157),

TCGA-LAML (n = 132), and TARGET-AML (n = 181). All RNA-seq data were converted to transcripts per million (TPM) format to improve comparability across different datasets. Count data were downloaded from the TCGA for differential expression analysis, and 70 normal control samples were obtained from the Genotype-Tissue Expression (GTEx) project (<https://xenabrowser.net/datapages/>).

An independent in-house cohort from Ruijin Hospital, comprising both RNA-seq data and comprehensive clinical annotations, was also used as an external validation dataset. This dataset was obtained directly from Dr. Peng Jin with appropriate authorization. Part of this cohort has been uploaded to the GEO database (GSE201492), while the full dataset used in this study has been previously described and processed in Dr. Jin's published work [38–40].

Identification of ER stress-related cell death genes

We retrieved ER stress-related genes by searching the keyword “ER stress” on the GeneCards website (GeneCards—Human Genes | Gene Database | Gene Search). Genes with a relevance score below 5 were filtered out, resulting in a final set of 1,363 ER stress-related genes used for subsequent analyses. Thirteen patterns of different PCD genes were extracted from three previous studies [41–43] and reputable scientific databases, including gene set enrichment analysis (GSEA) gene sets, Kyoto Encyclopedia of Genes and Genomes (KEGG) and FerriDb. After eliminating duplicate genes, the following 2,773 PCD-related genes were obtained: intrinsic apoptosis (n = 579), extrinsic apoptosis (n = 354), ferroptosis (n = 399), cuproptosis (n = 28), entotic cell death (n = 9), autophagy (n = 673), lysosome-dependent cell death (n = 71), netotic cell death (n = 6), necroptosis (n = 289), alkaliptosis (n = 9), pyroptosis (n = 258), parthanatos (n = 28), and immunogenic cell death (n = 70). The “DESeq2” package was used to identify differentially expressed genes (DEGs) in TCGA-LAML and GTEx normal bone marrow samples [44]. A log₂-fold change (log₂ FC) greater than 1 and a false discovery rate (FDR) of less than 0.05 were set as the thresholds for identifying DEGs. In the subsequent step, we performed an intersection analysis of the DEGs, ER stress-related genes, and cell death-related genes and visualized the results via a Venn diagram. Additionally, Pearson correlation analysis was conducted on the RNA-seq data from the GSE37642 samples to identify genes coexpressed between ER stress and PCD, with a correlation coefficient (R) greater than 0.6 and a P value (P) less than 0.05.

Establishment of the prognostic model

We first partitioned the data into separate training and validation sets to construct a predictive model with stability and accuracy. Given its relatively large sample size, the GSE37642 dataset was selected as the training set, and the other three published datasets (GSE12417, TCGA-LAML, and TARGET-AML) were used for internal validation. Initially, a univariate Cox regression analysis was performed on the training set to identify genes that exhibited a significant association with prognosis, specifically those with an adjusted p value less than 0.05. We subsequently employed the “Mime” R package, which integrates 10 machine learning algorithms (including random survival forest (RSF), elastic network (Enet), stepwise Cox regression (StepCox), Cox model with boosting algorithm (CoxBoost), least absolute shrinkage and selection operator (Lasso), ridge regression (Ridge), partial least squares regression for survival (plsRcox), survival support vector machine (survival-SVM), generalized boosted regression modeling (GBM), and supervised principal components (SuperPC)), and 117 algorithm combinations to select variables and develop the prognostic model in training set GSE37642 [45]. We applied tenfold cross-validation to mitigate potential overfitting during model development. Specifically, the training dataset was randomly partitioned into 10 equal-sized folds. In each iteration, nine folds were used for model training, and the remaining one was used for validation. This process was repeated 10 times, allowing each fold to serve once as a validation set. This cross-validation procedure was applied consistently to all the algorithmic combinations to ensure fair comparison. All the constructed models were evaluated in the three validation cohorts. For each model, Harrell’s concordance index (C-index) was calculated across all datasets, and the model with the highest average C-index was selected to calculate the ERCDI for every AML patient in the training and validation cohorts. In this study, the combination of StepCox [both] and Enet [$\alpha = 0.2$] achieved the highest average C-index and was selected as the final prognostic model. The ERCDI was calculated as follows:

$$\text{ERCDI} = \sum_1^i (\text{Coef}_i * \text{ExpGene}_i),$$

where i represents the model gene, Coef denotes the regression coefficient, and ExpGene indicates the corresponding gene expression level. Then, according to the median value of the ERCDI, the patients in each cohort were classified into high-risk and low-risk groups, with those having an ERCDI above the median assigned to the high-risk group and those with scores below the median assigned to the low-risk group. Finally, Kaplan–Meier

curves were generated to evaluate the prognostic significance of the model, and ROC curves were generated to assess its efficacy.

Development and assessment of the nomogram model

Univariate and multivariate Cox regression analyses were performed to confirm whether the ERCDI is an independent prognostic predictor for AML patients. The multivariate analysis incorporated several established clinical variables, including age, FAB, Runx1.Runx1 t1_fusion, and Runx1_mutation, allowing us to evaluate the prognostic value of ERCDI beyond traditional factors. The “rms” package was subsequently utilized to develop a nomogram according to the Cox regression results to systematically evaluate the survival probability of individual patients. To evaluate the nomogram’s predictive accuracy and clinical utility, we generated calibration plots to compare the predicted and observed survival probabilities and performed decision curve analysis (DCA) to assess the net clinical benefit across a range of threshold probabilities.

Unsupervised consensus clustering and GO enrichment analysis

The “ConsensusClusterPlus” R package was utilized to identify different molecular subtypes of patients according to the ER stress-related cell death gene (ERCDG) expression profile [46]. The partitioning around medoids (PAM) algorithm was applied, and the Pearson distance was calculated. A total of 1000 resampling iterations were conducted (reps = 1000), with 80% of the samples randomly selected in each iteration (pItem = 0.8), to ensure the robustness and stability of the clustering results. The optimal number of clusters was determined through the consensus matrix, cumulative distribution function (CDF), and relative change in the area under the CDF curve. Subsequently, Kaplan–Meier survival analysis was performed to compare the overall survival (OS) probability of each molecular subtype. A Sankey diagram was generated to illustrate the associations among molecular subtypes, the ERCDI, and survival status. GO enrichment analysis was conducted to clarify the functional characteristics of each molecular subtype.

Assessment of the TME

Cell-type Identification by Estimating Relative Subpopulations of RNA Transcripts (CIBESORT) and single-sample gene set enrichment analysis (ssGSEA) algorithms were employed to evaluate differences in immune cell infiltration between the high- and low-risk groups [47, 48]. Pearson correlation analysis was performed to examine the associations between ERCDI signature genes and immune cells or immune checkpoint-related genes. The

“Estimation of Stromal and Immune Cells in Malignant Tumor Tissues Using Expression Data” (ESTIMATE) algorithm was utilized to compare immune, stromal, and ESTIMATE scores between different risk groups [49].

Chemotherapy sensitivity and immunotherapy response analysis

The “OncoPredict” package is a useful tool for predicting individual sensitivity to various chemotherapy drugs [50]. We employed this algorithm to calculate the half-maximal inhibitory concentration (IC₅₀) values of several common chemotherapy drugs for each AML patient. The Tumor Immune Dysfunction and Exclusion (TIDE) website was used for immunotherapy response prediction, and the TIDE score was calculated [51].

Cell lines and cell culture

Human AML cell lines (U937 and HL60) were purchased from DSMZ. The cells were cultured in RPMI-1640 supplemented with 10% FBS at 37 °C with 5% CO₂. The cell density was controlled between 5×10^5 cells/mL and 2×10^6 cells/mL. Mycoplasma testing was performed, and no contamination was observed.

Reagents

Cytarabine, doxorubicin, venetoclax, PIK-75, and panobinostat (LBH589) were obtained from Selleck Chemicals. Prutenin and chaetocin were purchased from Felixbio.

Lentivirus-mediated gene knockdown

Target sequences (TGATGCCTAGCCAGTTGGTAA#1 and GTGTAGCATGTACCTTATTAT#1) against human DDIT4 and a control scrambled sequence (GCGCGCTTTGTAGGATTCGTT) were inserted into the PLKO.1 vector according to the manufacturer’s protocol (Addgene, Watertown, MA, USA). The generated lentivirus carrying short hairpin RNA (shRNA) was used to infect target cells for 48 h, after which the cells were subjected to puromycin selection at 2 µg/mL.

Immunoblot analysis

Total cellular proteins were extracted with RIPA lysis buffer (Epizyme) supplemented with protease and phosphatase inhibitors. After thorough lysis, the lysates were centrifuged at $12,000 \times g$ at 4 °C for 15 min. The supernatant was collected, transferred to another new centrifuge tube, and denatured for 10 min at 100 °C. The protein samples were subsequently separated via SDS-PAGE and transferred to 0.45 µm PVDF membranes. The membranes were blocked in a protein-free rapid-blocking solution before being incubated overnight at 4 °C with the primary antibody. After being washed three times with PBST, the membranes were incubated with

the corresponding secondary antibodies. The immunoblot signals were acquired with an Amersham Imager 600 (General Electric Company, Boston, MA, USA). The primary antibodies used for the western blotting assays were rabbit antibodies against DDIT4 (1:1000, 10638-1-AP; Proteintech, Wuhan, Beijing) and mouse antibodies against beta-actin (1:1000, AC004; ABClonal Technology, Wuhan, China).

Cell proliferation, the cell cycle, and apoptosis

Cell proliferation was analyzed via a CCK-8 kit and a cell counting assay. Briefly, 5×10^4 cells were seeded in 96-well plates, and after 24, 48, and 72 h, 10 µL of CCK-8 solution was added to each well, and the absorbance at 450 nm was measured after 2.5 h of incubation. The number of cells at different time points was calculated via Countess II (AMQAX1000, Thermo Fisher Scientific). An APC BrdU Flow Kit (BD Pharmingen) was used to detect the percentages of different cell cycle phases (G0G1, S, and G2/M). Apoptosis was assessed via an Annexin-V Apoptosis Detection Kit (BioLegend, CA, USA). The data produced by the flow cytometer were analyzed via FlowJo software.

Colony formation assay

A 100 µL cell suspension with a density of 5×10^5 cells/mL was mixed with 1 mL of methylcellulose semisolid medium and added to a 6-well cell culture plate. After mixing and spreading evenly, the plate was placed in a 37 °C incubator for static culture. Colony formation was considered positive when there were ≥ 50 cells per colony. The number of colonies was counted after 10 days.

Migration and invasion assays

A 24-well Transwell system (TCS003024, Biofil) was utilized to conduct migration and invasion assays. Briefly, a 200 µL cell suspension containing 1×10^5 cells in serum-free 1640 medium was added to the upper chamber of the well, and 500 µL of 1640 medium containing 20% FBS was added to the lower chamber. After 24 h of incubation at 37 °C, the cells were fixed with 4% paraformaldehyde for 15 min and stained with 0.25% crystal violet for 30 min. The cells that remained in the upper chamber were photographed.

Animal models

NOD-SCID mice were purchased from GemPharmatech. A total of 9×10^6 Luciferase-mCherry-HL60 tumor cells were intravenously injected into the mice (6 weeks, female). The mice were allocated randomly into different experimental groups (4 groups [vehicle, venetoclax, chaetocin, and venetoclax + chaetocin], $n = 5$) and then intraperitoneally administered 30 mg/

kg venetoclax or 1 mg/kg chaetocin, individually or in combination, every other day for 3 weeks, beginning 10 days after the xenograft. A quantitative imaging system was used to monitor tumor growth. The mice were sacrificed by CO₂ inhalation when they became moribund. Animal care and sacrifice were conducted according to methods approved by the Animal Care and Use Committee of the Center for Animal Experiments of Shanghai Jiao Tong University.

Statistical analysis

Statistical analyses were performed using R software (version 4.4.0). For continuous variables, differences between two groups were assessed via a two-tailed Student's *t* test. The data were checked for normality and homogeneity of variance to meet the assumptions of parametric testing. The group means are displayed as histograms, with error bars representing the standard error of the mean (\pm SEM). For categorical variables, comparisons between groups were performed via the Chi-square test. Significance is indicated as follows: **P* < 0.05, ***P* < 0.01, or ****P* < 0.001.

Results

Preliminary identification of signatures related to ER stress and PCD

First, as shown in Fig. 1A, a total of 2773 genes from 13 distinct PCD patterns were collected. Differential expression analysis was subsequently performed between AML and normal samples from TCGA and GTEx, as depicted in Fig. 1B. We then conducted GO and KEGG analyses to identify the most significantly enriched pathways. The results revealed that many DEGs were involved in signaling pathways associated with protein import, cytokine interactions, major histocompatibility complex (MHC) assembly (Additional file 1: Figs. S1 A–B). GSEA was subsequently performed to identify ER stress and PCD pathway alterations. As shown in Fig. S1 C, ER stress and various PCD pathways, including apoptosis, autophagy, ferroptosis, necroptosis, and netotic cell death, were dysregulated in AML samples, suggesting their potential involvement in disease progression. We subsequently extracted all the ER stress- and PCD-related DEGs. As illustrated in the Venn diagram (Fig. 1C), 1565 PCD-related genes and 690 ER stress genes were identified as differentially expressed. Next, Pearson correlation analysis was performed on these genes to identify common signatures involved in ER stress and cell death processes. Using screening criteria of $r > 0.6$ and *P* < 0.05, 121 ER stress-related genes and 413 PCD-related genes

were identified as co-expressed genes (Additional file 5: Table S1). Univariate Cox regression analysis was then applied to select genes associated with patient prognosis, and 23 genes with a *P* value < 0.05 were identified for further analysis.

Construction of the ERCDI for predicting AML patient prognosis using a machine-learning combinatorial algorithm

According to the expression profiles of 23 genes, we applied the “Mime” R package to evaluate the prognostic performance of 117 algorithm combinations. GSE37642 was used as the training cohort, whereas the other 3 cohorts served as validation cohorts. The average C-index across the four cohorts was used as the criterion for model selection. Ultimately, the step Cox + Enet ($\alpha = 0.2$) algorithm combination emerged as the optimal model with the highest average C-index across all four cohorts. We then applied these two algorithms for model gene selection and construction, identifying the top 9 genes with the highest variable importance (Fig. 1E, F). The coefficient values for each gene are depicted in Fig. 1G. The ERCDI was subsequently calculated via the following formula: $\text{ERCDI} = (0.31 \times \text{DSG2 exp}) + (0.24 \times \text{IL2RA exp}) + (0.23 \times \text{HSPA2 exp}) + (0.19 \times \text{GLO1 exp}) + (0.17 \times \text{DDIT4 exp}) + (0.13 \times \text{IGF2BP3 exp}) + (0.09 \times \text{ADM exp}) + (-0.41 \times \text{AGER}) + (-0.05 \times \text{MPO exp})$.

The patients in the different cohorts were stratified into high-risk and low-risk subgroups according to the median ERCDI. Compared with that in the low-risk group, the ERCDI in the high-risk group was generally greater. Kaplan–Meier curve analysis revealed that the overall survival time of patients in the high-risk group was shorter than that of patients in the low-risk group (Fig. 2B). The risk factor linkage plot also indicated that the proportion of deceased patients in the high-risk group was greater than that in the low-risk group (Fig. 2A). ROC curve analysis revealed high area under the curve (AUC) values for the prediction of the 1-, 3-, and 5-year survival rates of AML patients in both the training and validation cohorts (Fig. 2C).

Establishment and assessment of the nomogram model

Univariate and multivariate Cox regression analyses were conducted to better evaluate the predictive value of the ERCDI. As shown in Fig. 3A and B, ERCDI was an independent risk factor in both the univariate Cox regression (HR = 1.794, 95% CI: 1.601–2.010, *P* < 0.001) and multivariate Cox regression (HR = 1.581, 95% CI: 1.383–1.808, *P* < 0.001) analyses. A nomogram model was constructed via multivariate Cox and stepwise regression to predict the 1-, 3-, and 5-year OS rates of AML patients

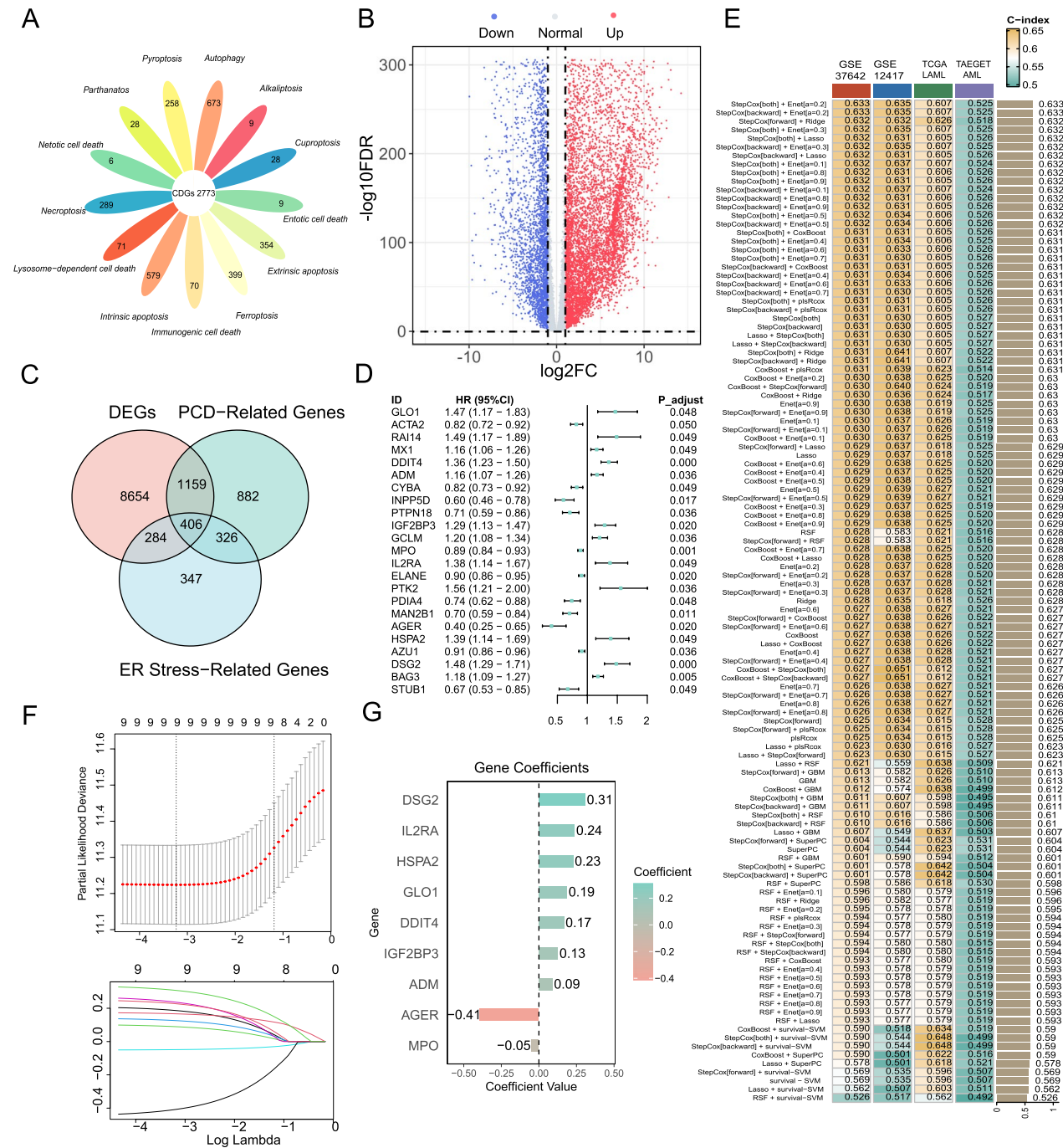


Fig. 1 Identification of ERCDGs and machine learning-based construction of the ERCDI. **A** Collection of key regulatory genes containing 13 PCD patterns. **B** Identification of differentially expressed genes. Differentially expressed genes between normal bone marrow and AML tissues. **C** A total of 690 ER stress-related genes and 1,565 programmed cell death-associated genes were identified as differentially expressed genes. **D** Univariate Cox analysis of 534 co-expressed genes. **E** The 117 machine-learning algorithms used for unicon analysis-related genes; the c-index of each model was calculated. **F** Cross-validation of the ERCDI signature constructed via LASSO regression. The optimal λ was obtained when the partial likelihood of deviance reached the minimum value. **G** Coefficient values of the ERCDGs in the Step Cox + Enet [$\alpha = 0.2$] model

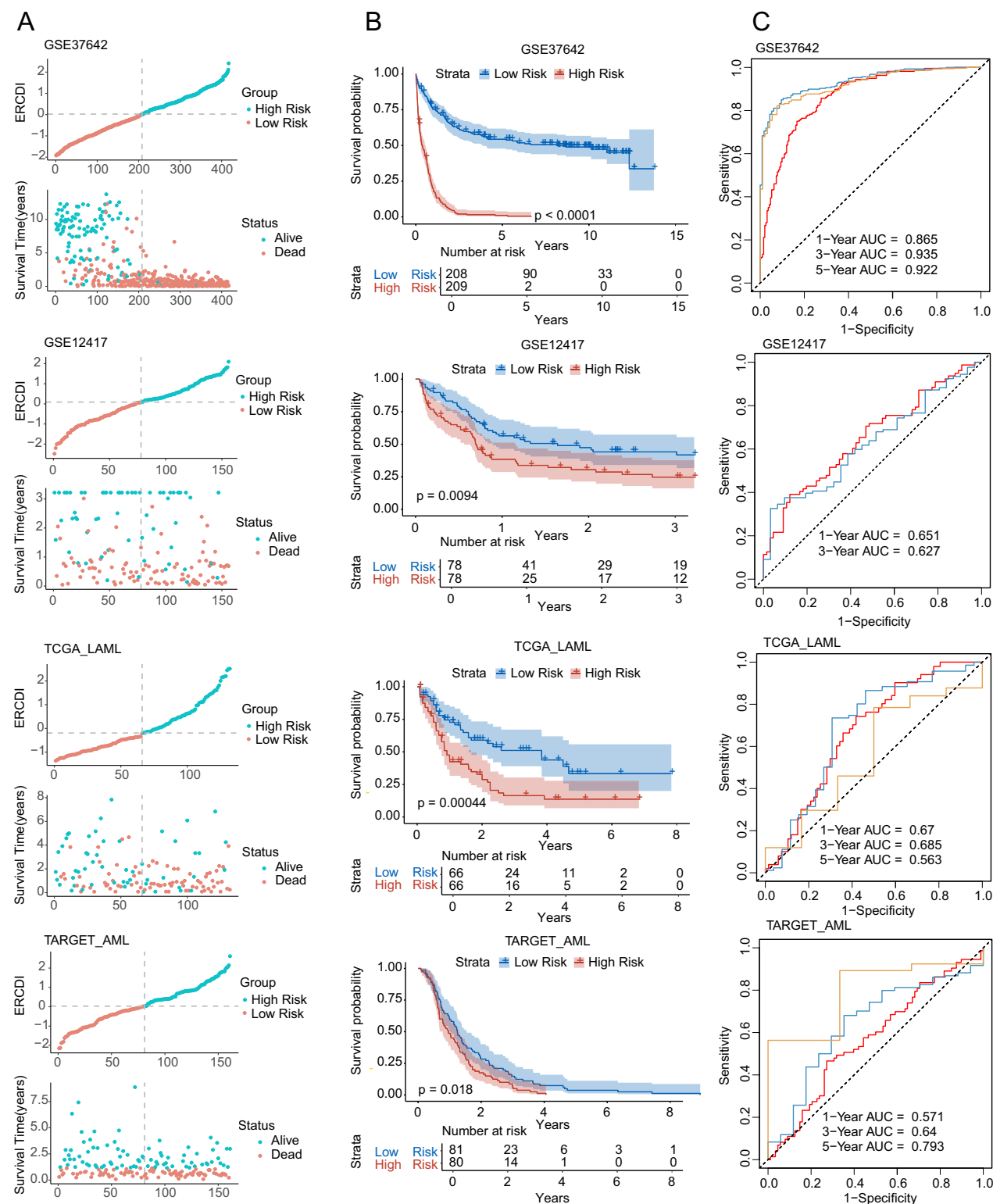


Fig. 2 Internal training and validation of the gene signature prediction model. **A** Distribution of the ERCDI according to survival status and time in the GSE37642, GSE12417, TCGA-LAML, and TARGET-AML cohorts. **B** OS of patients in the low- and high-ERCDI groups in the GSE37642, GSE12417, TCGA-LAML, and TARGET-AML cohorts. **C** ROC analysis of the ability of the ERCDI to predict 1-, 3-, and 5-year overall survival outcomes in the GSE37642, GSE12417, TCGA-LAML, and TARGET-AML cohorts

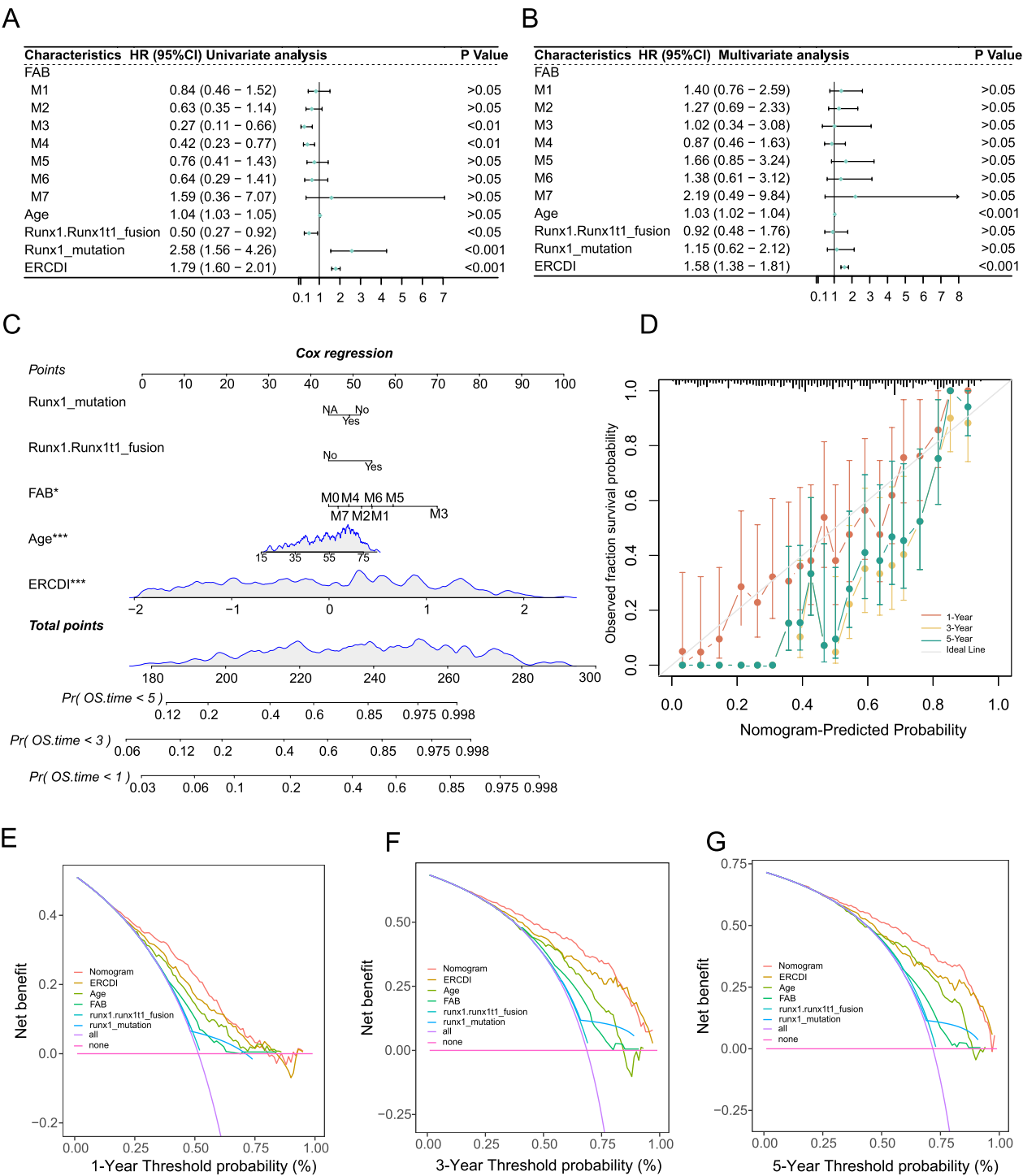


Fig. 3 Establishment and assessment of the nomogram survival model. **A** Univariate analysis of the clinicopathologic characteristics and ERCDI in the GSE37642 cohort. **B** Multivariate analysis of the clinicopathologic characteristics and ERCDI in the GSE37642 cohort. **C** Establishment of a nomogram model based on clinicopathologic characteristics and the ERCDI. **D** Calibration plots showing the probabilities of 1-, 3-, and 5-year overall survival in the GSE37642 cohort. **E–G** Decision curve analysis (DCA) of a nomogram for predicting 1-, 3-, and 5-year overall survival

(Fig. 3C). Calibration curves revealed that the nomogram model accurately predicted the mortality rates of AML patients at different time points (Fig. 3D). Furthermore, DCA revealed that our nomogram model demonstrated notable net benefits across a wide spectrum of risks (Fig. 3E–G).

Comparison of gene expression-based prognostic signatures in AML

In recent years, advancements in next-generation sequencing and big-data analytics have facilitated the

development of numerous prognostic models according to gene expression profiles. To evaluate the predictive performance of our ERCDI model, we selected four well-established and classic prognostic signatures for AML as comparators: the inflammation-associated gene score (iScore) [12], immune dysfunction signature (PI20) [13], leukemia stem cell score (LSC17) [9] and AML-specific risk genes (GENE4) [52]. We conducted univariate Cox regression across all datasets for each signature and then calculated the corresponding C-index. The ERCDI notably displayed a higher C-index than the other models did

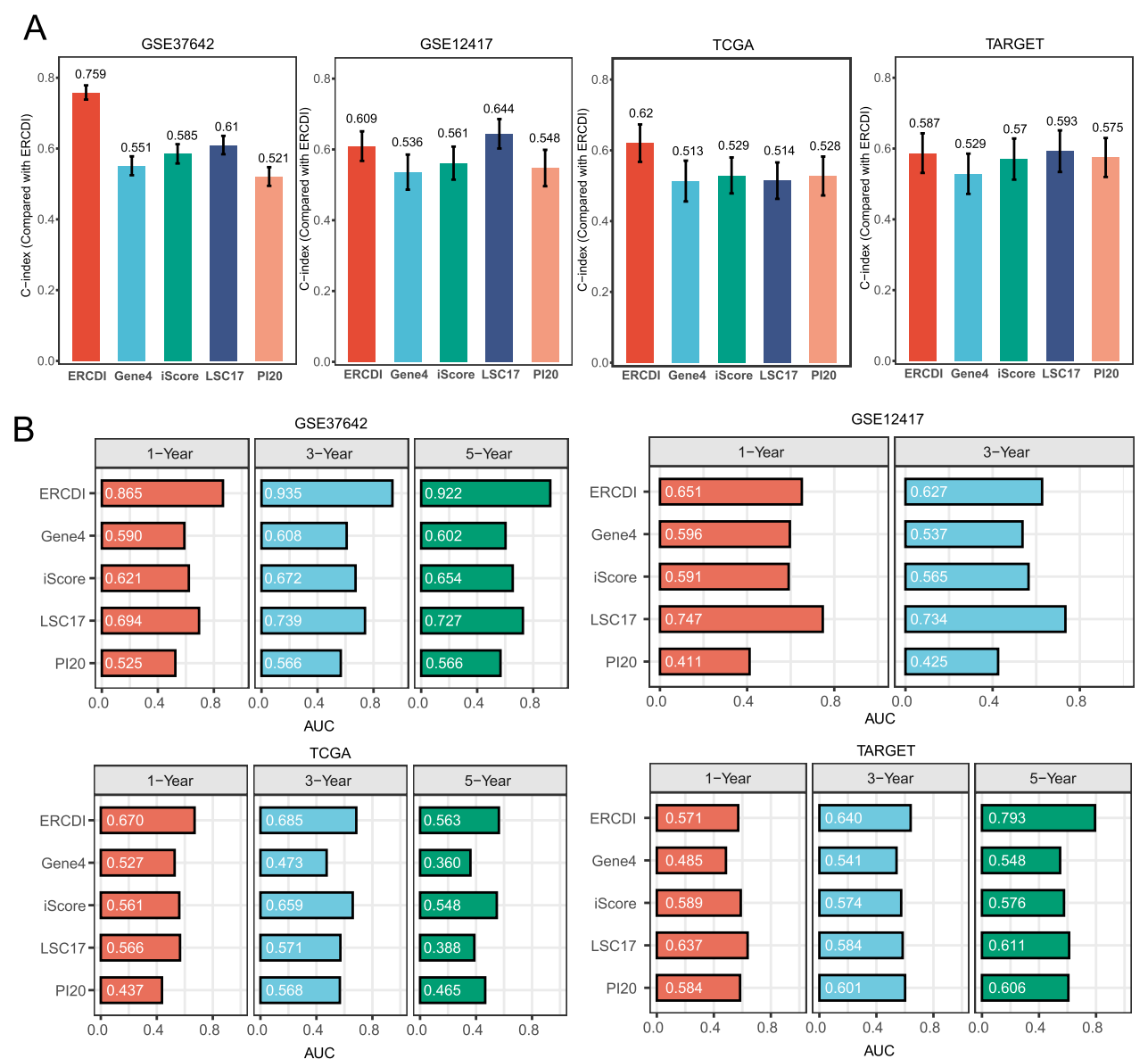


Fig. 4 Comparison of gene expression-based prognostic signatures in AML. **A** C-index analysis ERCDI and four published risk models in the GSE37642, GSE12417, TCGA-LAML, and TARGET-AML cohorts. **B** Time-dependent ROC analysis for predicting overall survival outcomes at 1, 3, and 5 years. The data are presented as the means ± 95% confidence intervals (CIs)

in the GSE37642 and TCGA cohorts, albeit with slightly lower performance than LSC17 in the GSE12417 cohort. In the TARGET cohort, all five predictive models demonstrated comparable predictive power, with the ERCDI and LSC17 marginally ahead (Fig. 4A).

To facilitate a more comprehensive comparison, we subsequently performed a time-dependent ROC analysis for each model to evaluate its performance in predicting OS rates at 1, 3, and 5 years across all cohorts. The ERCDI consistently demonstrated superior predictive accuracy in most cohorts and time points, with the exception of the GSE12417 cohort, where LSC17 proved superior (Fig. 4B). In summary, these findings highlight that the ERCDI is a potent and reliable prognostic indicator that is independent of previously published gene expression-based models and holds promise for risk stratification in AML patients.

External validation of the ERCDI model in a clinical in-house cohort

To further assess the clinical applicability of our ERCDI model as a practical tool, we utilized an in-house cohort from Ruijin Hospital to evaluate its predictive performance and robustness in a real-world clinical setting. As shown in Fig. 5A and B, AML patients stratified into high-risk groups by ERCDI exhibited worse overall survival and higher mortality rates. The AUCs of our model for predicting 1- and 3-year OS rates were 0.650 and 0.722, respectively (Fig. 5C). Moreover, patients in the high-risk group also exhibited shorter event-free survival (EFS) durations than those in the low-risk group, further supporting the clinical utility of our model (Fig. 5D). Finally, we compared the performance of the ERCDI model with that of four other existing prognostic models in the RJAML cohort. While the C-index indicated that the predictive ability of the ERCDI was slightly lower than that of the LSC17 (Fig. 5E), time-dependent ROC analysis demonstrated that the predictive performance

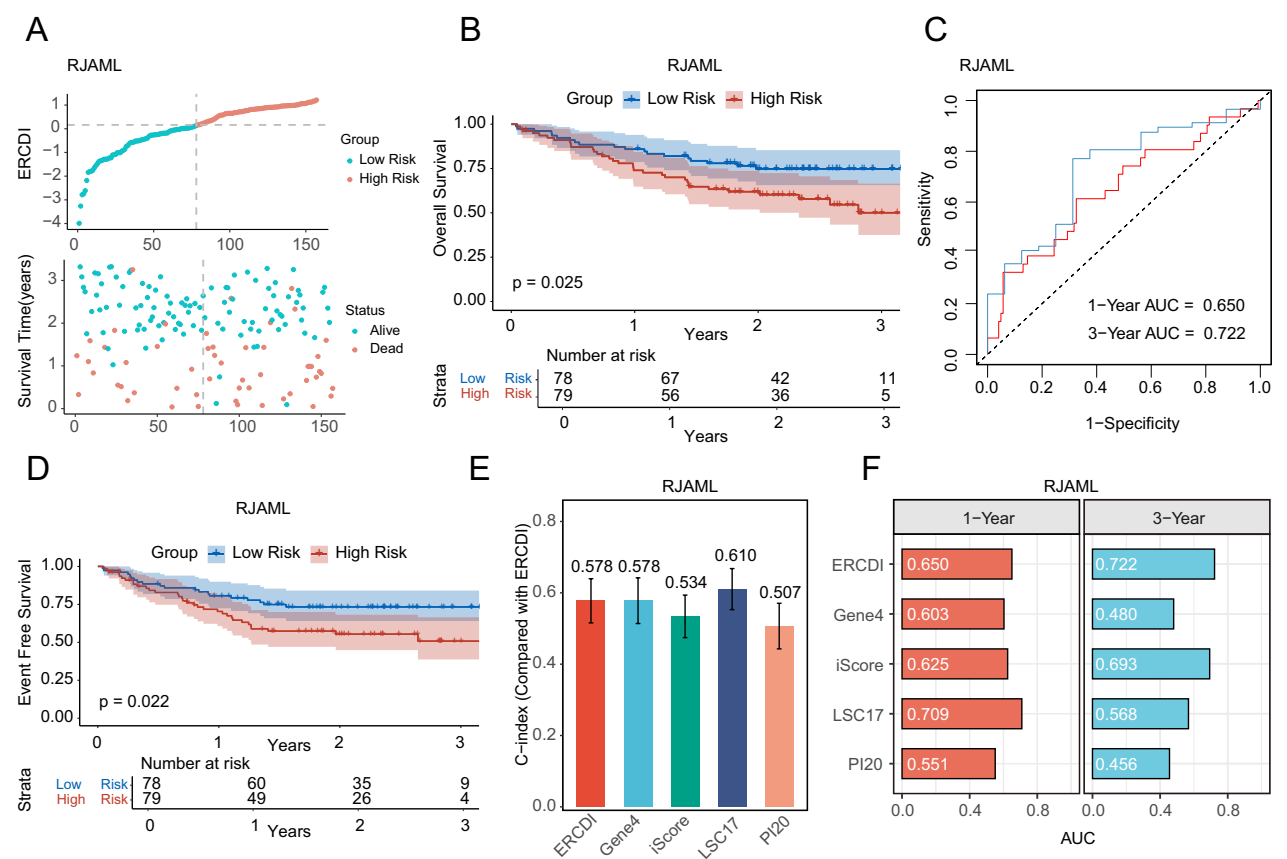


Fig. 5 External validation of the ERCDI model in a clinical in-house cohort. **A** Distribution of ERCDI according to survival status and time in the RJAML cohort. **B** Overall survival of patients in the low- and high-ERCDI groups in the RJAML cohort. **C** ROC analysis of the ability of the ERCDI to predict 1- and 3-year overall survival outcomes. **D** Kaplan–Meier curves of EFS according to the ERCDI in RJAML. **E** C-index analysis of the ERCDI and four published risk models in RJAML. **F** Time-dependent ROC analysis for predicting overall survival outcomes at 1 and 3 years

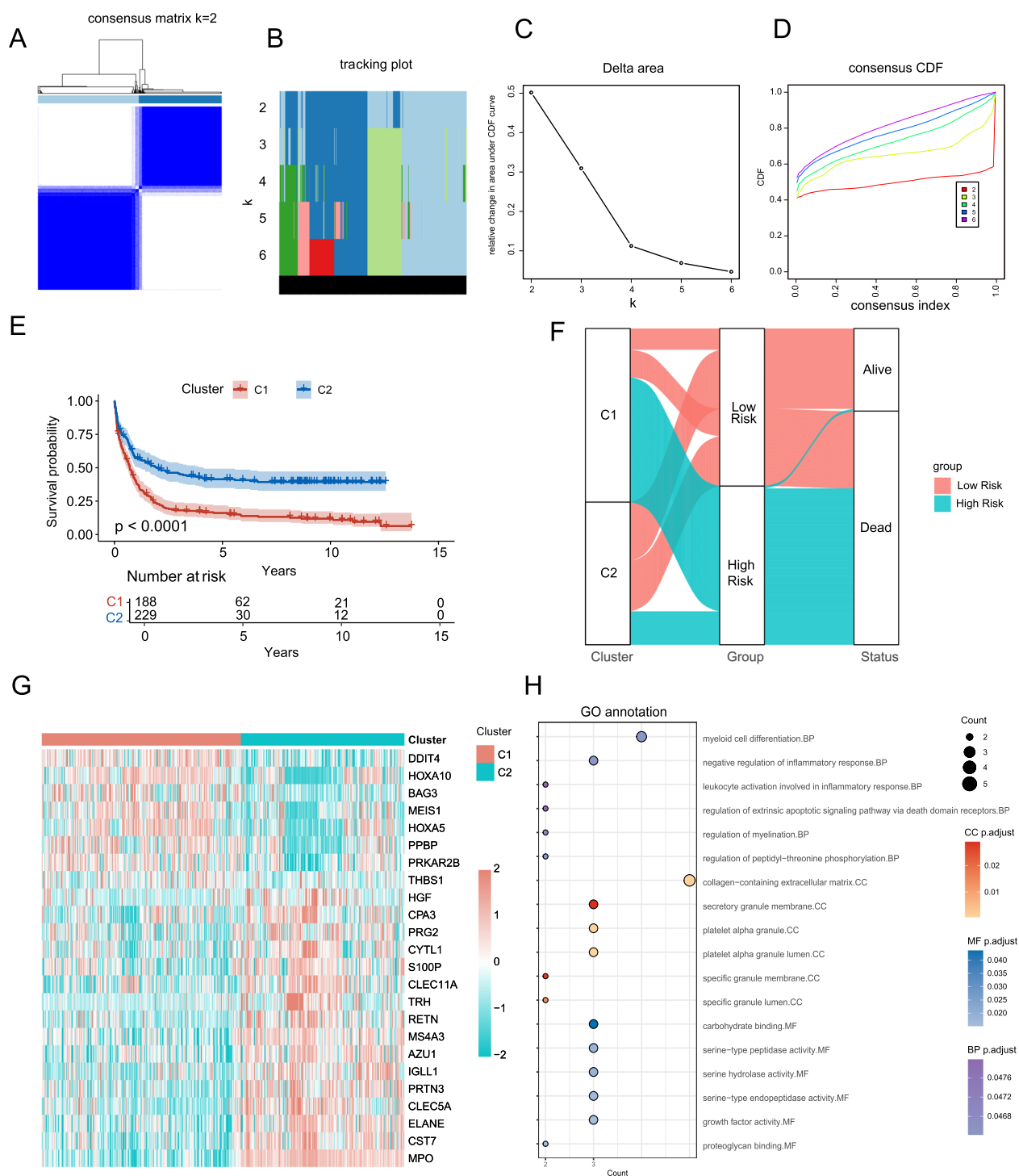


Fig. 6 Clusters of ERCDGs and their biological characteristics in AML. **A** Consensus matrix of the GSE37642 cohort for k = 2; **B** the sample distribution changed with k values from 2 to 6; **C**, the relative change in area under the CDF curve; **D** CDF with k values from 2 to 6. **E** Kaplan–Meier analysis of the prognosis of patients in the two molecular clusters in the GSE37642 cohort. **F** Alluvial diagram showing the interrelationship between molecular clusters, survival status, and ERCDI groups in AML patients. **G** DEGs between the two molecular clusters. **H** GO annotation of the genes shown in Fig. 4G

of the ERCDI improved over time and eventually outperformed the other four models (Fig. 5F).

Development of ERCDI-related molecular subtypes

Consensus clustering analysis was performed to explore the relationship between ERCDI signature genes and the development of AML. Owing to the low crossover in the consensus matrix, the lack of a significant shift in the area under the curve, and the uniform trend in the cumulative distribution function (CDF) (Fig. 6A–D), two distinct molecular subtypes ($k = 2$) were identified. Kaplan–Meier curve analysis revealed that the overall survival time of patients in cluster 1 was significantly shorter than that of patients in cluster 2 (Fig. 6E). Similarly, the alluvial diagrams revealed that most patients in cluster 1 were in the high-risk group, indicating a greater ERCDI, whereas the opposite trend was observed in cluster 2 (Fig. 6F). Differential analysis between the two clusters revealed that two ERCDI signature genes, DDIT4 and MPO, were differentially expressed, with DDIT4 expression upregulated in cluster 1 and MPO expression upregulated in cluster 2 (Fig. 6G). According to the GO analysis, the main functions of these DEGs were associated with myeloid cell differentiation, negative regulation of the inflammatory response, leukocyte activation involved in the inflammatory response, and other processes (Fig. 6H), suggesting a strong correlation with the immune system.

Analysis of the TME between different risk groups

In light of the aforementioned findings, we hypothesized the existence of distinct differences in the immune microenvironment between the high-risk and low-risk groups. To investigate this hypothesis, we employed the CIBERSORT algorithm to assess immune cell infiltration between the two ERCDI groups. The high-risk group exhibited fewer antitumor immune cells, such as memory B cells, CD8 + T cells, regulatory T cells (Tregs), and NK cells, but greater naïve B cell, dendritic cell, and resting mast cell infiltration (Fig. 7A). Subsequently, Spearman correlation analysis was performed, with additional validation by another algorithm, ssGSEA, which yielded similar results (Additional file 2: Fig S2). Moreover, the expression levels of key immune checkpoints were examined. Several genes, such as CXCL10, IL10, and TNFSF9, demonstrated upregulated expression in the high-risk group, whereas the expression of others, including BTN3A1 and TGFB1, was downregulated (Fig. 7B and C). Additionally, we utilized the ESTIMATE algorithm to evaluate the immune score, ESTIMATE score, stromal score, and tumor purity in the two risk groups. Compared with the low-risk group, the high-risk group had higher immune scores, ESTIMATE scores, and stromal scores, but lower tumor purity (Fig. 7D–G).

Correlation of the ERCDI with chemosensitivity and immunotherapy responses

To explore the relationship between the model and drug sensitivity, we utilized “oncoPredict” analysis to calculate IC50 values for several common drugs used to treat AML in both the high- and low-risk groups. As shown in Fig. 8A, the ERCDI value was positively correlated with the IC50 values of most drugs, suggesting that patients in the high-risk group are more likely to experience a poor response to chemotherapy. Additionally, we conducted a more intuitive comparison of several classical and promising drugs for treating AML. We observed that the high-risk group exhibited increased resistance to cytarabine, vorinostat, venetoclax, navitoclax, EPZ5676, and fludarabine, as indicated by higher IC50 values, while demonstrating greater sensitivity to other agents, such as mitoxantrone and dasatinib, reflected by their lower IC50 values (Fig. 8B). These results suggest differing chemosensitivity between the two risk groups.

Next, we applied the TIDE algorithm to predict individual immunotherapy responses in different risk groups. The TIDE score was calculated, and the median value was greater in the high-risk group than in the low-risk group, indicating a lower degree of therapeutic benefit from immunotherapy (Fig. 8C). Pearson correlation analysis also revealed a positive relationship between the TIDE score and the ERCDI (Fig. 8D). Correspondingly, a stacked bar chart revealed that patients in the low-risk group were more likely to respond to immunotherapy than those in the high-risk group were, as depicted in Fig. 8E.

The ERCDI signature gene DDIT4 influences the proliferation and cell cycle of AML cells

In subsequent studies, we aimed to identify potential AML targets from the 9 ERCDI signatures. We first analyzed the impact of these genes on OS on the basis of gene expression levels. We found that all the genes significantly influenced the OS time, with three genes—DSG2, DDIT4, and MPO—showing more convincing results, with $P < 0.0001$ (Additional file 3: Fig S3 A). The Mime package, which integrates 117 algorithms, identified 9 genes exhibiting the most significant effects across all algorithms, including 6 ERCDI genes, namely, DDIT4, HSPA2, GLO1, DSG2, AGER, and MPO, with DDIT4 being the most frequently identified gene (Additional file 3: Figs. S3B, C). Moreover, as shown in Fig. 6G, the DDIT4 and MPO genes were differentially expressed across the different groups, and high DDIT4 expression was associated with poor prognosis. Researchers have previously employed bioinformatics methods to explore the impact of high DDIT4 expression on the survival of AML patients; however, strong experimental evidence

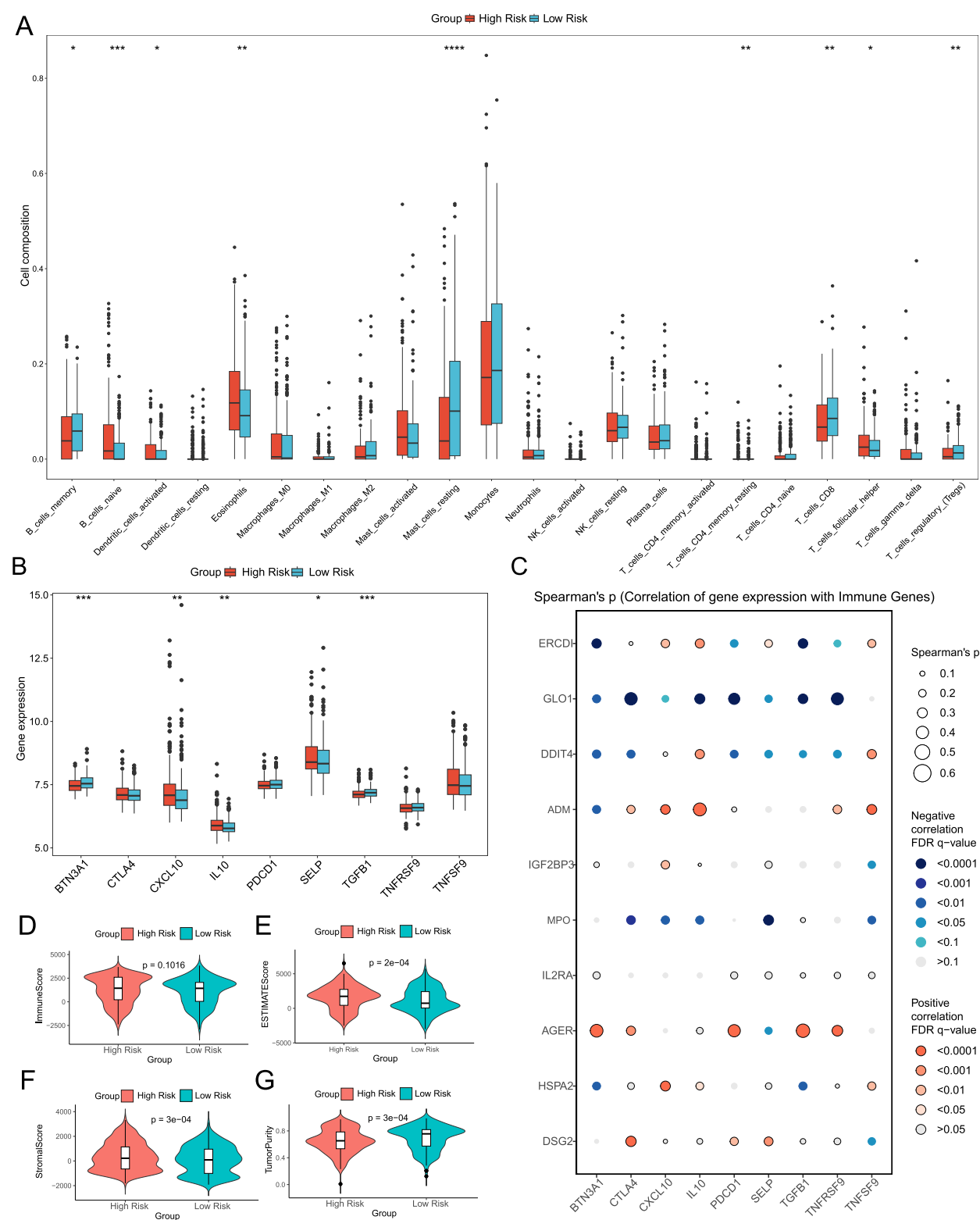


Fig. 7 Molecular and immune profiling of the ERCDI subgroups. **A, B** Differences in immune cell infiltration (**A**) and immune checkpoint expression (**B**) between different risk groups in the GSE37642 cohort. **C** Bubble plot of the relationships among immune checkpoint genes, the ERCDI, and model genes. **D–G** Violin plots comparing the immune score (**D**), ESTIMATES score (**E**), Stromal score (**F**), and tumor purity (**G**) between the high- and low-risk groups

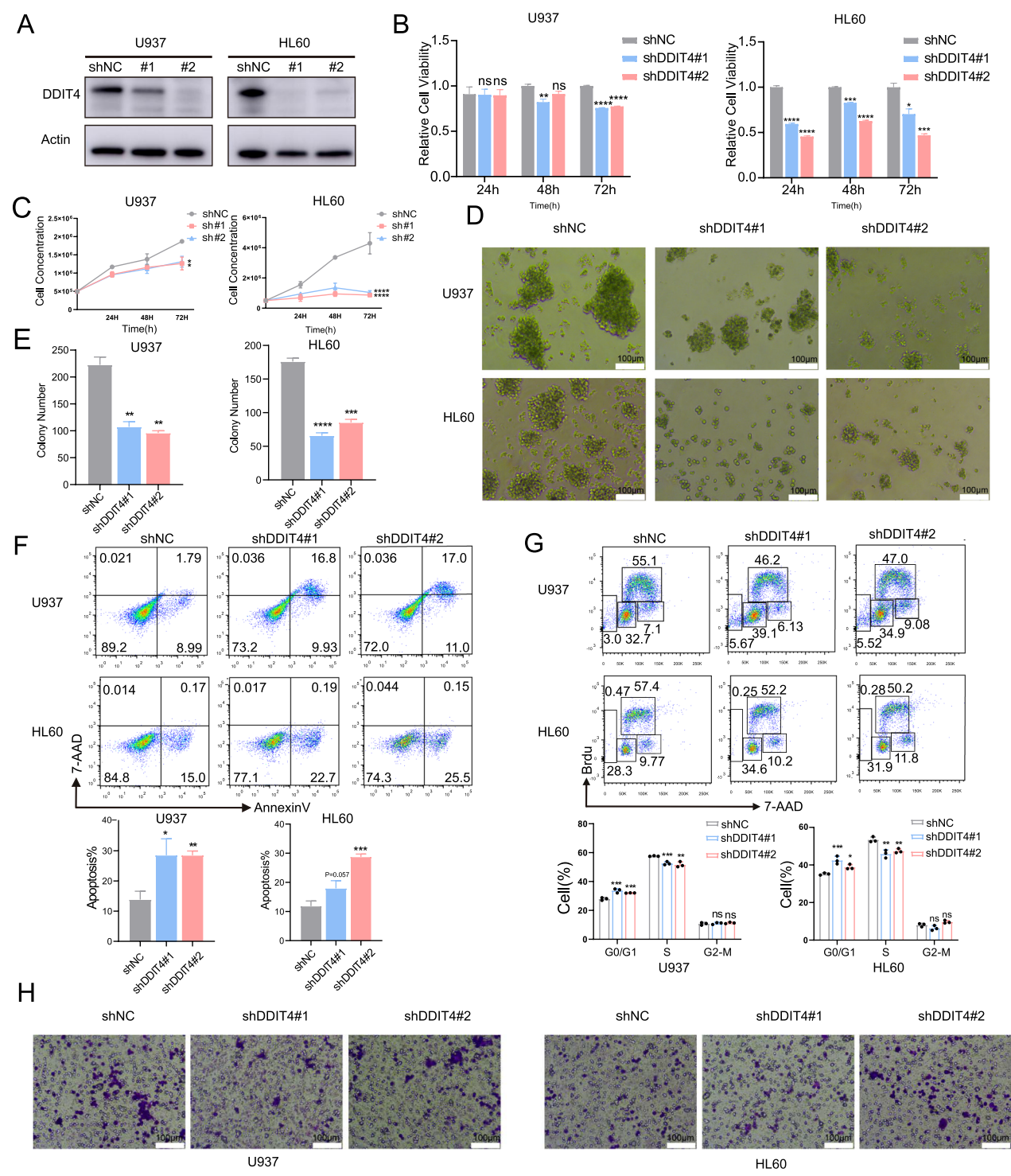


Fig. 9 DDIT4 promotes AML cell proliferation in vitro. **A** Knockdown of DDIT4 in U937 and HL60 cell lines. **B–H** Analysis of cell viability (**B**), cell counting (**C**), colony formation (**D–E**), cell apoptosis (**F**), the cell cycle (**G**), and migration (**H**) in control and DDIT4-knockdown cells. * $P < 0.05$, ** $P < 0.01$, *** $P < 0.001$

cell lines, U937 and HL60 (Fig. 9A). A previous study revealed that DDIT4 positively affects tumor proliferation in gastric cancer [45]. Similarly, DDIT4 knockdown significantly inhibited AML cell proliferation (Fig. 9B, C). Additionally, the colony formation assay results indicated that the proliferative function of AML cells was impaired (Fig. 9D, E). Furthermore, the percentage of apoptotic cells increased following DDIT4 knockdown (Fig. 9F). Cell cycle analysis was also performed, as DDIT4 is an essential factor in DNA quality control. The results showed that the knockdown of DDIT4 decreased the fraction of cells in the S phase (which reflects the proliferation rate) and induced G0/G1 arrest (Fig. 9G), consistent with the results of the previous proliferative function analysis. However, the migration ability of AML cells did not appear to be affected after DDIT4 knockdown (Fig. 9H). In summary, DDIT4 may play an important role in the progression of AML.

Screening of potential anti-AML drugs using the CMap database and a novel combined therapeutic strategy

Currently, chemotherapy remains the primary therapeutic approach for treating AML. However, resistance to chemotherapeutic agents is a significant challenge in clinical practice. Therefore, the development of new drugs and the exploration of novel combination therapies are crucial. In this study, we utilized the CMap database to identify potential therapeutic agents. The top 50 upregulated and downregulated DEGs from the high- and low-risk groups were uploaded to the database (Fig. 10A). The top 4 compounds (prunetin, PIK-75, chaetocin, and panobinostat) with negative scores ≤ -90 (Fig. 10B) were identified, suggesting potential antitumor effects. We then performed *in vitro* and *in vivo* experiments to evaluate the efficacy of the four compounds. First, CCK-8 assays were performed to calculate the IC₅₀. The results revealed that the IC₅₀ values of each drug, except for prunetin, were below 1 μ M (Fig. 10C, D). Therefore, the other three reagents were selected for subsequent studies. Given that the IC₅₀ values of these 3 drugs were all below 200 nM and that PIK-75 and panobinostat have narrow therapeutic windows, we selected values representing half of the IC₅₀ as the working concentration. First, we tested the ability of the drugs to induce apoptosis in AML cells. Interestingly, U937 cells were not as sensitive to either PIK-75 or panobinostat when treated with half of the IC₅₀ concentration (Fig. 10E). In HL60 cells, the apoptosis rates were similar when they were treated with the three drugs individually (Fig. 10E). According to the drug sensitivity results shown in Fig. 8, patients in the high-risk group exhibited poor responses to many chemotherapeutic agents, especially the BCL-2 inhibitor venetoclax, which is commonly used for elderly, unfit, or

chemotherapy-intolerant AML patients. Additionally, we observed that patients in the high-risk group were more resistant to cytarabine (Fig. 8B), the most frequently used drug and cornerstone of standard AML chemotherapy. Currently, combination therapy is a common strategy for treating AML. Therefore, we investigated whether combining these three compounds with two classical chemotherapeutic drugs could have a synergistic effect. We found that the apoptosis rate was significantly increased when chaetocin was combined with venetoclax, particularly in HL60 cells (Fig. 10F). Moreover, chaetocin can also be used in combination with cytarabine (Additional file 4: Fig. S4 A). For the other two compounds, a slight synergistic effect was observed when PIK-75 was combined with venetoclax, whereas no significant effect was observed with panobinostat (Additional file 4: Fig. S4B–C). On the basis of these findings, we propose that the combined use of chaetocin and venetoclax may represent a promising treatment strategy for AML. We then established a cell line-derived xenograft (CDX) model to assess the *in vivo* efficacy of our combination strategy using chaetocin and venetoclax. A low-dose monotherapy regimen was employed to minimize the risk of toxicity associated with combination therapies. Tumor growth was monitored via a quantitative imaging system. As shown in Fig. 10G, H, minimal inhibition of leukemia progression was observed in the single agent treatment group, whereas combination therapy notably delayed tumor progression. Similarly, the median survival time in the combination treatment group was significantly longer than that in the control or single agent treatment groups (Fig. 10I). In summary, our combination strategy demonstrated substantial therapeutic potential both *in vitro* and *in vivo*.

Discussion

AML is a complex hematopoietic malignancy characterized by diverse molecular alterations [1, 4]. The intricate pathogenesis and significant heterogeneity of AML complicate the development of effective treatment strategies, and accurately predicting the prognosis of individual AML patients remains a challenge. Currently, somatic mutations and cytogenetic abnormalities serve as the primary indicators for risk classification, which forms the cornerstone of ELN risk stratification [3]. As our understanding of AML biology deepens, novel prognostic factors and markers are being identified to refine prognostication and therapeutic strategies [53, 54]. Additionally, machine-learning techniques offer promising insights into predicting patient outcomes. However, the effective integration of these methods into clinical practice remains challenging. Key considerations for their implementation include selecting the appropriate

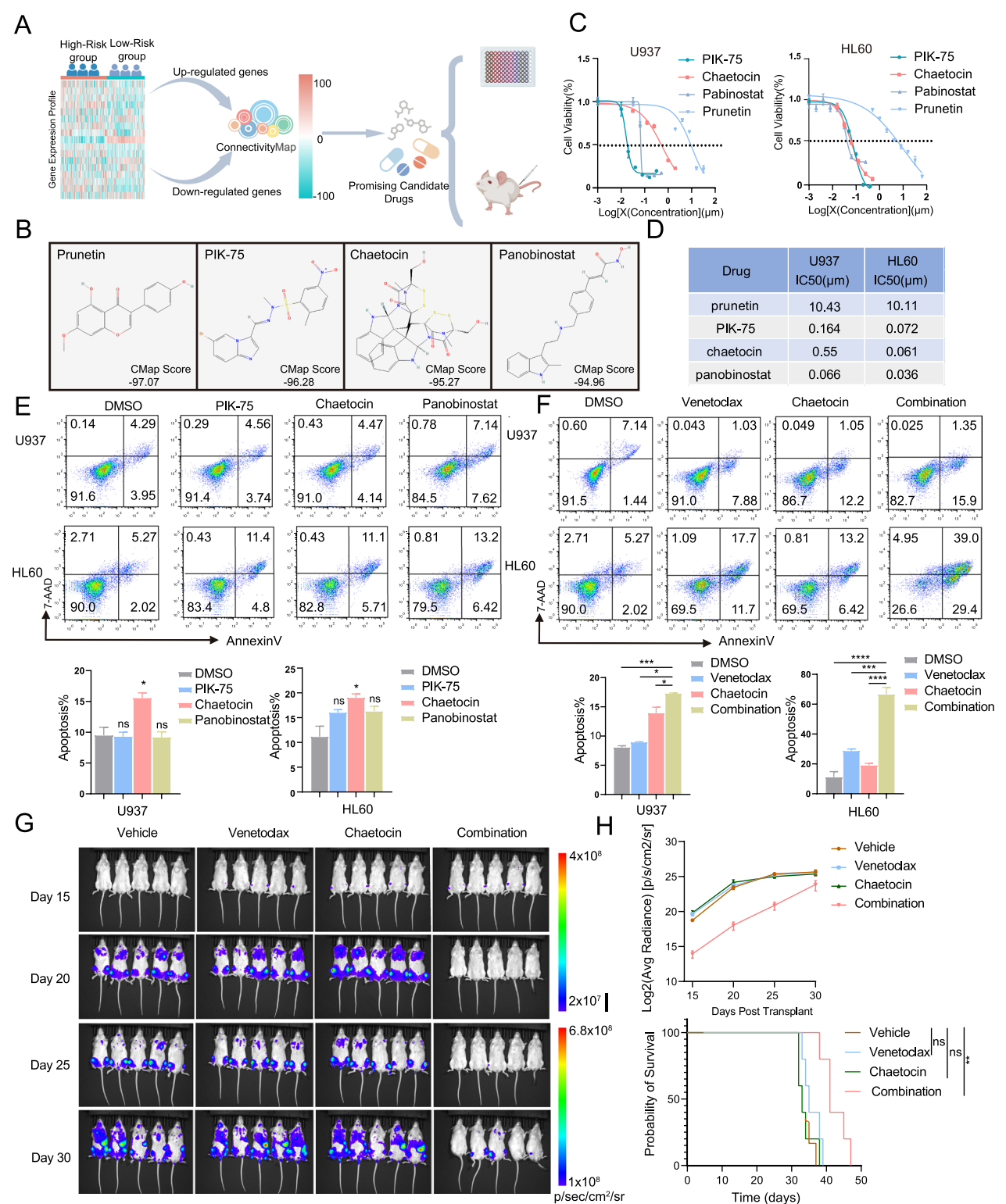


Fig. 10 The combined use of chaetocin and venetoclax has anti-AML effects both in vitro and in vivo. **Schematic** showing steps for identifying potential anti-AML drugs on the basis of the CMap database. **B** Molecular structural formulas of the top 4 small-molecule compounds with CMap scores less than −90. **C, D** IC50 values of four small-molecule compounds in U937 and HL60 cells according to the CCK-8 assay. **E** Twenty-four-hour apoptosis rates of U937 and HL60 cells after treatment with the four individual compounds. **F** Twenty-four-hour apoptosis rate of U937 and HL60 cells after treatment with chaetocin and venetoclax individually or in combination. **G, H** Representative bioluminescence images of tumor growth over time in the CDX mouse model (n = 5 per group). **I** Survival curves of the mice in each different group. * $P < 0.05$, ** $P < 0.01$, *** $P < 0.001$

machine learning algorithm and defining the specific application scenarios [45]. In recent years, dysregulated ER stress has been widely reported in various tumors and contributes greatly to many aspects of cellular processes, including metabolic pathways, inflammatory responses, and PCD mechanisms.

In this study, we utilized bioinformatics tools for the first time to explore the relationship between ER stress and cell death pathways and developed a prognostic model, the ERCDI, via a machine-learning framework. Our findings indicate that the ERCDI is an independent prognostic factor for AML. Furthermore, the ERCDI, TME, and drug sensitivity correlations suggest that the ERCDI may help elucidate the molecular mechanisms underlying AML progression. Using our model and the CMap database, we also identified a novel combination strategy for treating AML patients, emphasizing the potential clinical application of the ERCDI in screening potential therapeutic strategies. Our ERCDI model was established on the basis of 9 genes (DSG2, IL2RA, HSPA2, GLO1, DDIT4, IGF2BP3, ADM, AGER, and MPO) highly predictive of patient survival outcomes. Kaplan–Meier survival analysis revealed that AML patients with higher expression levels of AGER and MPO exhibited improved overall survival rates, whereas those with higher expression levels of desmoglein-2 (DSG2), interleukin-2 receptor subunit alpha (IL2RA), heat shock protein A2 (HSPA2), glyoxalase 1 (GLO1), DDIT4, insulin-like growth factor 2 mRNA-binding protein 3 (IGF2BP3), and adrenomedullin (ADM) presented shorter survival times. DSG2 is a cadherin family member and plays an important role in cell adhesion [55]. IL2RA forms the IL2 receptor complex with IL2RB and IL2RG [56]. IL2RA is expressed mainly in regulatory T cells. However, upregulated expression of IL2RA was also found in LSCs, which has been found to promote AML cell proliferation and predict a poor prognosis [56]. HSPA2 belongs to the HSP family and acts as a molecular chaperone to help maintain cellular homeostasis during various forms of environmental stress [57]. GLO1 belongs to the glyoxalase system, which detoxifies methylglyoxal (MG), thus playing an important role in cellular metabolism [58]. IGF2BP3 is recognized as an m6 A-binding protein [59]. Elevated expression of IGF2BP3 has been reported in AML patients and contributes to the survival of AML cells [60]. ADM, an important peptide responsible for the regulation of blood pressure, has been found to promote tumor growth in various types of cancers, including AML. Targeting ADM receptors might provide new therapeutic insight for cancer treatment [61]. Advanced glycosylation end product-specific receptor (AGER) is a type of cell surface receptor that correlates

with advanced glycation end products (AGEs) [62]. It is also the target of many other ligands, including high-mobility group box-1 (HMGB1), amyloid β peptides, and S100 proteins, which implies its involvement in the inflammatory response [63]. Myeloperoxidase (MPO) serves as an important biomarker of neutrophils and is involved in the antibactericidal response. Recently, overexpressed MPO has been reported to be associated with chemoresistance to cytarabine in some AML cell lines [64, 65].

DDIT4 is a cellular stress-responsive protein that acts as an internal inhibitor of the mTORC1 complex [66]. Its expression is upregulated under various stress conditions, including hypoxia, ER stress, and ionizing radiation [67]. Studies have demonstrated elevated DDIT4 expression in multiple tumor types, such as breast, lung, colon, ovarian, and gastric cancers and AML [68–70]. Higher DDIT4 expression has been associated with poor prognosis in several cancers, including lung and breast cancer and AML; however, the opposite effect has been observed in other cancers, such as gastric cancer and lower-grade glioma [67]. DDIT4 also influences tumor cell drug sensitivity. By inhibiting mTORC1 signaling, DDIT4 promotes resistance to temozolomide and radiotherapy in glioblastoma [71]. Additionally, DDIT4 mediates autophagosome–lysosome fusion by binding to CCAAT/enhancer-binding protein beta, leading to bortezomib resistance in prostate cancer [72]. In summary, the role of DDIT4 in tumor progression is complex. While *in silico* studies have linked higher DDIT4 expression to poor prognosis in AML, its precise molecular function remains to be fully elucidated. In this study, we demonstrated that elevated DDIT4 expression predicts poor survival in AML patients, which is consistent with previous reports [73]. We further explored the role of DDIT4 in AML through a series of *in vitro* experiments, revealing that DDIT4 knockdown suppresses AML cell proliferation and increases apoptosis, with concomitant G0/G1 phase cell cycle arrest. These findings suggest that DDIT4 may serve as a biomarker for AML prognosis and treatment.

The TME comprises various cell types, including tumor, stromal, and immune cells [74]. The complex interactions among these cells significantly influence tumor development. Our study revealed distinct immune cell compositions between the high- and low-ERCDI groups. Notably, the high-ERCDI group exhibited lower infiltration of antitumor immune cells, such as B cells, CD4 + T cells, and CD8 + T cells, indicating a more immunosuppressed phenotype [75]. In contrast, the low-ERCDI group, which has a better prognosis, had higher immune scores and tumor purity. This paradox suggests that an aggressive TME may also contribute to disease progression [76].

We further investigated the ability of the ERCDI to predict sensitivity to immunotherapy and chemotherapy. Using the TIDE algorithm, we found that patients in the high-risk group, as classified by the ERCDI, exhibited greater immunotherapy resistance than those in the low-risk group. These patients had higher TIDE scores, indicating a positive correlation between ERCDI and immune evasion. Regarding chemotherapy, high-risk patients showed increased resistance to commonly used therapeutic agents, particularly BCL-2 inhibitors such as venetoclax and navitoclax. These findings suggest that the ERCDI could serve as a predictive marker for personalized treatment selection for AML patients. Our results highlighted the importance of identifying potential therapeutic drugs for AML patients. Thus, we employed the CMap database to screen for candidate compounds and selected the top four. In vitro experiments confirmed that all four compounds inhibited the growth of AML cell lines, with chaetocin showing the most potent effect. Chaetocin is a naturally occurring compound isolated from *Chaetomium* fungi [77]. It was first regarded as a special inhibitor of the histone lysine methyltransferase SUV39H1 [78]. However, recent studies have demonstrated that chaetocin can induce cell apoptosis via many additional mechanisms, including the accumulation of ROS, DNA damage, and the activation of ER stress [79]. The potential role of chaetocin in cancer therapy has been reported for several malignancies, including gastric cancer, glioma, melanoma, and leukemia [77]. However, further research is needed to explore its clinical applications and elucidate the underlying mechanisms involved. In our study, we observed that patients in the high-risk group were more resistant to various chemotherapeutic drugs than were those in the low-risk group, with combined chemotherapy remaining the primary therapeutic strategy for AML [80]. Thus, we assessed the combined effects of chaetocin and two clinically used drugs, cytarabine and venetoclax. We found that the combination of chaetocin and venetoclax strongly affected the induction of cell apoptosis. This finding was further confirmed in an in vivo mouse model. Venetoclax is a selective inhibitor of BCL-2 that prevents it from binding and sequestering proapoptotic proteins such as BCL-2 Interacting Mediator of Cell Death (BIM), BCL-2-associated agonist of cell death (BAD), and P53 upregulated modulator of apoptosis (PUMA). This release of proapoptotic proteins triggers the mitochondrial apoptosis pathway, resulting in cell death [70]. Venetoclax has emerged as one of the most promising agents for targeted therapy in AML. However, its efficacy can be limited by mutations or overexpression of other BCL-2 family proteins, such as Mcl-1 and Bcl-xl, which can compensate for the inhibition of BCL-2 [81]. Additionally, venetoclax has a

narrow therapeutic window, which increases the risk of toxicity. As a result, combining venetoclax with other agents is a common strategy [82]. Classic combination therapies include hypomethylating agents (HMAs), FLT3 inhibitors, and IDH inhibitors [83]. Nevertheless, chemotherapy resistance frequently occurs. Therefore, exploring new combination drugs is necessary. In our study, we found that the percentage of apoptotic AML cells significantly increased following the combination of chaetocin and venetoclax. Notably, the doses used were considerably lower than those typically used for each drug, suggesting that our combination strategy offers lower toxicity and greater safety.

Several limitations of our study should be acknowledged. First, the ERCDI was developed using retrospective data, which necessitates prospective studies to confirm the clinical applicability of our model. Given the complex nature and diverse molecular subtypes of AML, further comparative investigations are needed to explore the role of ERCDI signatures in the progression of this disease. In addition, our analysis relied largely on bulk RNA-seq data. Considering the substantial intratumor heterogeneity features of AML, this approach may miss several features of important subclones, such as therapy-resistant populations or leukemic-regenerating cells. More importantly, the expression profiles of ER stress and PCD signals might vary or even be completely opposite across different cellular subtypes. Therefore, incorporating single-cell transcriptomic analyses in future studies might provide a more nuanced understanding of the molecular dynamics underlying AML.

Moreover, owing to sample size limitations, we collectively analyzed AML patients with diverse cytogenetic backgrounds. This may have led to the underrepresentation of gene signatures associated with rare karyotypes and introduced bias in model performance. Because treatment responses and clinical outcomes differ widely across AML subtypes, expanding the dataset and validating the model in stratified patient cohorts will be essential for improving its clinical applicability and precision. Finally, although we identified the potential of DDIT4 as a biomarker for AML and proposed a novel combination treatment strategy involving chaetocin and venetoclax, we did not perform in-depth mechanistic investigations. Furthermore, the proposed therapeutic approach currently lacks supporting clinical validation. Additional studies are needed to elucidate the remaining mechanisms and further assess this combination's translational potential in clinical settings.

Conclusions

In this study, we employed machine learning algorithms to establish a novel prognostic model using ER stress-related PCD genes and validated the model's predictive efficacy across multiple AML cohorts. We also identified DDIT4, an ERCDI signature, as a potential therapeutic target in AML. Furthermore, we proposed a new therapeutic strategy involving the combination of chaetocin and venetoclax, which might provide new insights for clinical treatment for AML patients.

Abbreviations

AML	Acute myeloid leukemia
ER stress	Endoplasmic reticulum stress
ERCDI	ER stress-related cell death index
HSCT	Hematopoietic stem cell transplantation
UPR	Unfolded protein response
IRE1α	Inositol-requiring enzyme 1α
XBP1	X-box binding protein 1
PERK	Protein kinase RNA-like endoplasmic reticulum kinase
ATF4	Activating transcription factor 4
eIF2α	Eukaryotic translation initiation factor 2α
ROC	Receiver operating characteristic curve
DDIT4	DNA damage-inducible transcript 4 protein
ELN	European LeukemiaNet
LSC	Leukemia stem cells
CHOP	C/EBP homologous protein
Bip	Binding-immunoglobulin protein
BI-1	Bax inhibitor-1
PTP-1B	Protein tyrosine phosphatase 1B
AIP1	ASK1-interacting protein 1
BMME	He bone marrow microenvironment
DAMPs	Damage-associated molecular patterns
CRT	Calreticulin
HSP70	Heat shock protein 70
ICD	Immunogenic cell death
TPM	Transcripts per million
GSEA	Gene set enrichment analysis
KEGG	Kyoto Encyclopedia of Genes and Genomes
DEGs	Differentially expressed genes
C-index	Harrell's concordance index
TCGA	The Cancer Genome Atlas
GEO	Gene expression omnibus
TARGET	Therapeutically applicable research to generate effective treatment
TME	The Tumor microenvironment
ERCDG	ER stress-related cell death gene
OS	Overall survival
IC50	The half-maximal inhibitory concentration
MHC	Major histocompatibility complex
AUC	Area under the curve
EFS	Event-free survival
CDX	Cell line-derived xenograft
BCL-2	B-cell lymphoma-2
BIM	BCL-2 interacting mediator of cell death
BAD	BCL-2-associated agonist of cell death
PUMA	P53 up-regulated modulator of apoptosis
HMA	Hypomethylating agents

Supplementary Information

The online version contains supplementary material available at <https://doi.org/10.1186/s12967-025-06615-y>.

Additional file 1: Figure S1. Enrichment analysis of DEGs: Gene Ontology analysis of DEGs: KEGG analysis of DEGs: GSEA analysis of ER stress and PCD related pathways

Additional file 2: Figure S2. Bubble plot of the relationship between immune cells, ERCDI, and model genes based on the CIBERSORT and ssGSEA algorithms

Additional file 3: Figure S3. Exploration of 9 ERCDI signatures. Kaplan–Meier mortality line was calculated of OS between patients with high or low expression of the nine ERCDGs. Top 9 selected genes by Mime R package. Intersection of ERCDGs and Mime selected genes

Additional file 4: Figure S4. Different combination strategies of the three CMap screened compounds and classical AML chemotherapeutic drugs. 24 h apoptosis rate of U937 and HL60 cells after treatment with chaetocin and Cytarabine individually or combined. 24 h apoptosis rate of U937 and HL60 cells after treatment with PIK-75 and Cytarabine/Venetoclax individually or combined. 24 h apoptosis rate of U937 and HL60 cells after treatment with Panobinostat and Cytarabine/Venetoclax individually or combined. * $p < 0.05$, ** $p < 0.01$, *** $p < 0.001$

Additional file 5: Table S1. Pearson results of the co-expressed genes

Acknowledgements

All contributors to this study are included in the list of authors. We gratefully acknowledge the GEO TCGA, and TARGET database and the uploader of the datasets. And we thank Dr. Peng Jin for generously providing in-house cohort data. Specifically, MW thanks her friends Jinlan Long and Jing Lu for their personal encouragement.

Author contributions

HL and GH designed the study. MW and HX conducted the bioinformatic analysis, analyzed the data, and drafted the manuscript. XX, WZ, and ZH performed the animal experiments. CL, YZ, and YW performed cell experiments, and YY, SX, RP, RW and HZ reviewed and revised the manuscript. All authors contributed to the article and approved the submitted version.

Funding

This work was supported by the National Natural Science Foundation of China (82470154, 82100154, 82200245, 82104447), the Open Project Program of the National Research Center for Translational Medicine at Shanghai (TMSZ-2020-204 and NRCTM(SH)-2021-09), the Collaborative Innovation Center of Hematology, and the Samuel Waxman Cancer Research Foundation.

Data availability

Publicly available datasets were analyzed in this study. These data can be found at: <https://www.ncbi.nlm.nih.gov/gds/?term=GSE37642,GSE12417>; <https://www.cancer.gov/ccg/research/genome-sequencing/target> and <https://www.cancer.gov/tcga/>.

Declarations

Ethics approval and consent to participate

This study was reviewed and approved by the Ethics Committee of Ruijin Hospital, Shanghai Jiao Tong University School of Medicine, and was carried out in accordance with the National Institutes of Health Guide for the Care and Use of Laboratory Animals.

Consent for publication

Not applicable.

Competing interests

The authors declare that they have no competing interests.

Author details

¹Shanghai Institute of Hematology, State Key Laboratory of Medical Genomics, National Research Center for Translational Medicine at Shanghai, Ruijin Hospital, Shanghai Jiao Tong University School of Medicine, Shanghai, China. ²School of Life Sciences and Biotechnology, Shanghai Jiao Tong University, Shanghai, China. ³Department of Endocrine and Metabolic Diseases, Shanghai Institute of Endocrine and Metabolic Diseases, Ruijin Hospital, Shanghai Jiao Tong University School of Medicine, Shanghai 200025, China.

Received: 27 February 2025 Accepted: 14 May 2025
Published online: 21 May 2025

References

- Shimony S, Stahl M, Stone RM. Acute myeloid leukemia: 2023 update on diagnosis, risk-stratification, and management. *Am J Hematol*. 2023;98(3):502–26.
- DiNardo CD, Perl AE. Advances in patient care through increasingly individualized therapy. *Nat Rev Clin Oncol*. 2019;16(2):73–4.
- Tseng S, Lee M-E, Lin P-C. A review of childhood acute myeloid leukemia: diagnosis and novel treatment. *Pharmaceuticals*. 2023;16(11):1614.
- Kantarjian HM, DiNardo CD, Kadia TM, Daver NG, Altman JK, Stein EM, et al. Acute myeloid leukemia management and research in 2025. *CA Cancer J Clin*. 2025;75(1):46–67.
- Newell LF, Cook RJ. Advances in acute myeloid leukemia. *BMJ*. 2021;375:n2026.
- Short NJ, Konopleva M, Kadia TM, Borthakur G, Ravandi F, DiNardo CD, et al. Advances in the treatment of acute myeloid leukemia: new drugs and new challenges. *Cancer Discov*. 2020;10(4):506–25.
- Kayser S, Levis MJ. The clinical impact of the molecular landscape of acute myeloid leukemia. *Haematologica*. 2023;108(2):308–20.
- Döhner H, Wei AH, Appelbaum FR, Craddock C, DiNardo CD, Dombret H, et al. Diagnosis and management of AML in adults: 2022 recommendations from an international expert panel on behalf of the ELN. *Blood*. 2022;140(12):1345–77.
- Ng SW, Mitchell A, Kennedy JA, Chen WC, McLeod J, Ibrahimova N, et al. A 17-gene stemness score for rapid determination of risk in acute leukemia. *Nature*. 2016;540(7633):433–7.
- Farge T, Saland E, de Toni F, Aroua N, Hosseini M, Perry R, et al. Chemo-therapy-resistant human acute myeloid leukemia cells are not enriched for leukemic stem cells but require oxidative metabolism. *Cancer Discov*. 2017;7(7):716–35.
- Boyd AL, Aslostovar L, Reid J, Ye W, Tanasijevic B, Porras DP, et al. Identification of chemotherapy-induced leukemic-regenerating cells reveals a transient vulnerability of human AML recurrence. *Cancer Cell*. 2018;34(3):483–98.e5.
- Lasry A, Nadorp B, Fornerod M, Nicolet D, Wu H, Walker CJ, et al. An inflammatory state remodels the immune microenvironment and improves risk stratification in acute myeloid leukemia. *Nat Cancer*. 2023;4(1):27–42.
- Rutella S, Vadakekolathu J, Mazziotta F, Reeder S, Yau TO, Mukhopadhyay R, et al. Immune dysfunction signatures predict outcomes and define checkpoint blockade-unresponsive microenvironments in acute myeloid leukemia. *J Clin Invest*. 2022;132(21).
- Pavlova Natalya N, Thompson CB. The emerging hallmarks of cancer metabolism. *Cell Metab*. 2016;23(1):27–47.
- Zhang W, Shi Y, Oyang L, Cui S, Li S, Li J, et al. Endoplasmic reticulum stress—a key guardian in cancer. *Cell Death Discov*. 2024;10(1):343.
- Hetz C. The unfolded protein response: controlling cell fate decisions under ER stress and beyond. *Nat Rev Mol Cell Biol*. 2012;13(2):89–102.
- Hetz C, Papa FR. The unfolded protein response and cell fate control. *Mol Cell*. 2018;69(2):169–81.
- Chen X, Cubillos-Ruiz JR. Endoplasmic reticulum stress signals in the tumour and its microenvironment. *Nat Rev Cancer*. 2020;21(2):71–88.
- Bartoszewski S, Collawn JF. Unfolded protein response (UPR) integrated signaling networks determine cell fate during hypoxia. *Cell Mol Biol Lett*. 2020;25:18.
- Khateb A, Ronai ZA. Unfolded protein response in leukemia: from basic understanding to therapeutic opportunities. *Trends Cancer*. 2020;6(11):960–73.
- Liao H, Liu S, Ma Q, Huang H, Goel A, Torabian P, et al. Endoplasmic reticulum stress induced autophagy in cancer and its potential interactions with apoptosis and ferroptosis. *Biochim Biophys Acta Mol Cell Res*. 2025;1872(1): 119869.
- Bhardwaj M, Leli NM, Koumenis C, Amaravadi RK. Regulation of autophagy by canonical and non-canonical ER stress responses. *Semin Cancer Biol*. 2020;66:116–28.
- Gu F, Nguyễn DT, Stuiblé M, Dubé N, Tremblay ML, Chevet E. Protein-tyrosine phosphatase 1B potentiates IRE1 signaling during endoplasmic reticulum stress. *J Biol Chem*. 2004;279(48):49689–93.
- Liu L, Zhao M, Jin X, Ney G, Yang KB, Peng F, et al. Adaptive endoplasmic reticulum stress signalling via IRE1α-XBP1 preserves self-renewal of haematopoietic and pre-leukaemic stem cells. *Nat Cell Biol*. 2019;21(3):328–37.
- Śniegocka M, Liccardo F, Fazi F, Masciarelli S. Understanding ER homeostasis and the UPR to enhance treatment efficacy of acute myeloid leukemia. *Drug Resist Updat*. 2022;64: 100853.
- Lagadinou ED, Sach A, Callahan K, Rossi RM, Neering SJ, Minhajuddin M, et al. BCL-2 inhibition targets oxidative phosphorylation and selectively eradicates quiescent human leukemia stem cells. *Cell Stem Cell*. 2013;12(3):329–41.
- Diepstraten ST, Anderson MA, Czabotar PE, Lessene G, Strasser A, Kelly GL. The manipulation of apoptosis for cancer therapy using BH3-mimetic drugs. *Nat Rev Cancer*. 2022;22(1):45–64.
- Sun H, Lin DC, Guo X, Kharabi Masouleh B, Gery S, Cao Q, et al. Inhibition of IRE1α-driven pro-survival pathways is a promising therapeutic application in acute myeloid leukemia. *Oncotarget*. 2016;7(14):18736–49.
- Cai X, Gao L, Teng L, Ge J, Oo ZM, Kumar AR, et al. Runx1 deficiency decreases ribosome biogenesis and confers stress resistance to hematopoietic stem and progenitor cells. *Cell Stem Cell*. 2015;17(2):165–77.
- Urra H, Aravena R, González-Johnson L, Hetz C. The UPRising connection between endoplasmic reticulum stress and the tumor microenvironment. *Trends Cancer*. 2024;10(12):1161–73.
- Doron B, Abdelhamed S, Butler JT, Hashmi SK, Horton TM, Kurre P. Transmissible ER stress reconfigures the AML bone marrow compartment. *Leukemia*. 2019;33(4):918–30.
- Wang ES, Fay HRS, Dykstra KM, Phelps MN, Johnson M, Harrigan A, et al. Autophagy inhibition induces AML cell death and enhances the efficacy of chemotherapy under hypoxia. *bioRxiv*. 2024.
- Heydt Q, Larue C, Saland E, Bertoli S, Sarry JE, Besson A, et al. Oncogenic FLT3-ITD supports autophagy via ATF4 in acute myeloid leukemia. *Oncogene*. 2018;37(6):787–97.
- Chen X, Cubillos-Ruiz JR. Endoplasmic reticulum stress signals in the tumour and its microenvironment. *Nat Rev Cancer*. 2021;21(2):71–88.
- Fucikova J, Truxova I, Hensler M, Becht E, Kasikova L, Moserova I, et al. Calreticulin exposure by malignant blasts correlates with robust anticancer immunity and improved clinical outcome in AML patients. *Blood*. 2016;128(26):3113–24.
- Galluzzi L, Vitale I, Aaronson SA, Abrams JM, Adam D, Agostinis P, et al. Molecular mechanisms of cell death: recommendations of the Nomenclature Committee on Cell Death 2018. *Cell Death Differ*. 2018;25(3):486–541.
- Newton K, Strasser A, Kayagaki N, Dixit VM. Cell death. *Cell*. 2024;187(2):235–56.
- Jin P, Jin Q, Wang X, Zhao M, Dong F, Jiang G, et al. Large-scale in vitro and in vivo CRISPR-Cas9 knockout screens identify a 16-gene fitness score for improved risk assessment in acute myeloid leukemia. *Clin Cancer Res*. 2022;28(18):4033–44.
- Jiang G, Jin P, Xiao X, Shen J, Li R, Zhang Y, et al. Identification and validation of a novel CD8+ T cell-associated prognostic model based on ferroptosis in acute myeloid leukemia. *Front Immunol*. 2023;14:1149513.
- Li Z, Jin P, Xiang R, Li X, Shen J, He M, et al. A CD8(+) T cell related immune score predicts survival and refines the risk assessment in acute myeloid leukemia. *Front Immunol*. 2024;15:1408109.
- Zou Y, Xie J, Zheng S, Liu W, Tang Y, Tian W, et al. Leveraging diverse cell-death patterns to predict the prognosis and drug sensitivity of triple-negative breast cancer patients after surgery. *Int J Surg*. 2022;107: 106936.
- Qin H, Abulaiti A, Maimaiti A, Abulaiti Z, Fan G, Aili Y, et al. Integrated machine learning survival framework develops a prognostic model based on inter-crosstalk definition of mitochondrial function and cell death patterns in a large multicenter cohort for lower-grade glioma. *J Transl Med*. 2023;21(1):588.
- Cao K, Zhu J, Lu M, Zhang J, Yang Y, Ling X, et al. Analysis of multiple programmed cell death-related prognostic genes and functional validations of necroptosis-associated genes in oesophageal squamous cell carcinoma. *EBioMedicine*. 2024;99: 104920.

44. Love MI, Huber W, Anders S. Moderated estimation of fold change and dispersion for RNA-seq data with DESeq2. *Genome Biol.* 2014;15(12):550.
45. Liu H, Zhang W, Zhang Y, Adegboro AA, Fasoranti DO, Dai L, et al. Mime: a flexible machine-learning framework to construct and visualize models for clinical characteristics prediction and feature selection. *Comput Struct Biotechnol J.* 2024;23:2798–810.
46. Wilkerson MD, Hayes DN. ConsensusClusterPlus: a class discovery tool with confidence assessments and item tracking. *Bioinformatics.* 2010;26(12):1572–3.
47. Newman AM, Liu CL, Green MR, Gentles AJ, Feng W, Xu Y, et al. Robust enumeration of cell subsets from tissue expression profiles. *Nat Methods.* 2015;12(5):453–7.
48. Foroutan M, Bhuvana DD, Lyu R, Horan K, Cursons J, Davis MJ. Single sample scoring of molecular phenotypes. *BMC Bioinform.* 2018;19(1).
49. Yoshihara K, Shahmoradgolli M, Martínez E, Vegesna R, Kim H, Torres-García W, et al. Inferring tumour purity and stromal and immune cell admixture from expression data. *Nat Commun.* 2013;4(1).
50. Maeser D, Gruener RF, Huang RS. oncoPredict: an R package for predicting in vivo or cancer patient drug response and biomarkers from cell line screening data. *Briefings Bioinform.* 2021;22(6).
51. Fu J, Li K, Zhang W, Wan C, Zhang J, Jiang P, et al. Large-scale public data reuse to model immunotherapy response and resistance. *Genome Med.* 2020;12(1).
52. Chen Z, Song J, Wang W, Bai J, Zhang Y, Shi J, et al. A novel 4-mRNA signature predicts the overall survival in acute myeloid leukemia. *Am J Hematol.* 2021;96(11):1385–95.
53. Döhner H, Wei AH, Löwenberg B. Towards precision medicine for AML. *Nat Rev Clin Oncol.* 2021;18(9):577–90.
54. Hackl H, Astanina K, Wieser R. Molecular and genetic alterations associated with therapy resistance and relapse of acute myeloid leukemia. *J Hematol Oncol.* 2017;10(1).
55. Myo Min KK, French CB, McClure BJ, Ortiz M, Dorward EL, Samuel MS, et al. Desmoglein-2 as a cancer modulator: friend or foe? *Front Oncol.* 2023;13.
56. Nguyen CH, Schlerka A, Grandits AM, Koller E, van der Kouwe E, Vassiliou GS, et al. IL2RA promotes aggressiveness and stem cell-related properties of acute myeloid leukemia. *Can Res.* 2020;80(20):4527–39.
57. Scieglińska D, Krawczyk Z. Expression, function, and regulation of the testis-enriched heat shock HSPA2 gene in rodents and humans. *Cell Stress Chaperones.* 2015;20(2):221–35.
58. He Y, Zhou C, Huang M, Tang C, Liu X, Yue Y, et al. Glyoxalase system: a systematic review of its biological activity, related-diseases, screening methods and small molecule regulators. *Biomed Pharmacother.* 2020;131:110663.
59. Zhang N, Shen Y, Li H, Chen Y, Zhang P, Lou S, et al. The m6A reader IGF2BP3 promotes acute myeloid leukemia progression by enhancing RCC2 stability. *Exp Mol Med.* 2022;54(2):194–205.
60. Liu X, Chen J, Chen W, Xu Y, Shen Y, Xu X. Targeting IGF2BP3 in Cancer. *Int J Mol Sci.* 2023;24(11):9423.
61. Jailani ABA, Bigos KJA, Avgoustou P, Egan JL, Hathway RA, Skerry TM, et al. Targeting the adrenomedullin-2 receptor for the discovery and development of novel anti-cancer agents. *Expert Opin Drug Discov.* 2022;17(8):839–48.
62. Koerich S, Parreira GM, de Almeida DL, Vieira RP, de Oliveira ACP. Receptors for Advanced Glycation End Products (RAGE): promising targets aiming at the treatment of neurodegenerative conditions. *Curr Neuroparmacol.* 2023;21(2):219–34.
63. Rouhiainen A, Kuja-Panula J, Tumova S, Rauvala H. RAGE-mediated cell signaling. *Calcium-Binding Proteins and RAGE. Methods Mol Biol* 2013. p. 239–63.
64. Lin W, Chen H, Chen X, Guo C. The roles of neutrophil-derived myeloperoxidase (MPO) in diseases: the new progress. *Antioxidants.* 2024;13(1):132.
65. Hosseini M, Rezvani HR, Aroua N, Bosc C, Farge T, Saland E, et al. Targeting myeloperoxidase disrupts mitochondrial redox balance and overcomes cytarabine resistance in human acute myeloid leukemia. *Can Res.* 2019;79(20):5191–203.
66. Ellisen LW. mTOR Regulation through the REDD1-TSC Pathway. *Cell Cycle.* 2005.
67. Ding F, Gao F, Zhang S, Lv X, Chen Y, Liu Q. A review of the mechanism of DDIT4 serve as a mitochondrial related protein in tumor regulation. *Sci Prog.* 2021;104(1):36850421997273.
68. Britto FA, Dumas K, Giorgetti-Peraldi S, Ollendorff V, Favier FB. Is REDD1 a metabolic double agent? Lessons from physiology and pathology. *Am J Physiol Cell Physiol.* 2020;319(5):C807–24.
69. Tirado-Hurtado I, Fajardo W, Pinto JA. DNA damage inducible transcript 4 gene: the switch of the metabolism as potential target in cancer. *Front Oncol.* 2018;8.
70. Zoncu R, Efeyan A, Sabatini DM. mTOR: from growth signal integration to cancer, diabetes and ageing. *Nat Rev Mol Cell Biol.* 2010;12(1):21–35.
71. Foltyn M, Luger AL, Lorenz NI, Sauer B, Mittelbronn M, Harter PN, et al. The physiological mTOR complex 1 inhibitor DDIT4 mediates therapy resistance in glioblastoma. *Br J Cancer.* 2019;120(5):481–7.
72. Barakat DJ, Mendonça J, Barberi T, Zhang J, Kachhap SK, Paz-Priel I, et al. C/EBPβ regulates sensitivity to bortezomib in prostate cancer cells by inducing REDD1 and autophagosome-lysosome fusion. *Cancer Lett.* 2016;375(1):152–61.
73. Du F, Sun L, Chu Y, Li T, Lei C, Wang X, et al. DDIT4 promotes gastric cancer proliferation and tumorigenesis through the p53 and MAPK pathways. *Cancer Commun.* 2018;38(1):1–14.
74. Whiteside TL. The tumor microenvironment and its role in promoting tumor growth. *Oncogene.* 2008;27(45):5904–12.
75. Chen DS, Mellman I. Elements of cancer immunity and the cancer-immune set point. *Nature.* 2017;541(7637):321–30.
76. Li J, Byrne KT, Yan F, Yamazoe T, Chen Z, Baslan T, et al. Tumor cell-intrinsic factors underlie heterogeneity of immune cell infiltration and response to immunotherapy. *Immunity.* 2018;49(1):178–93.e7.
77. Jiang H, Li Y, Xiang X, Tang Z, Liu K, Su Q, et al. Chaetocin: A review of its anticancer potentials and mechanisms. *Eur J Pharmacol.* 2021;910:174459.
78. Xin DE, Liao Y, Rao R, Ogurek S, Sengupta S, Xin M, et al. Chaetocin-mediated SUV39H1 inhibition targets stemness and oncogenic networks of diffuse midline gliomas and synergizes with ONC201. *Neuro Oncol.* 2024;26(4):735–48.
79. Lian B, Lin Q, Tang W, Qi X, Li J. SUV39H1 is a new client protein of Hsp90 degraded by chaetocin as a novel C-terminal inhibitor of Hsp90. *Biomol Ther.* 2021;29(1):73–82.
80. Zhou C, Martinez E, Di Marcantonio D, Solanki-Patel N, Aghayev T, Peri S, et al. JUN is a key transcriptional regulator of the unfolded protein response in acute myeloid leukemia. *Leukemia.* 2016;31(5):1196–205.
81. Fowler-Shorten DJ, Hellmich C, Markham M, Bowles KM, Rushworth SA. BCL-2 inhibition in haematological malignancies: clinical application and complications. *Blood Rev.* 2024;65: 101195.
82. Hu M, Li W, Zhang Y, Liang C, Tan J, Wang Y. Venetoclax in adult acute myeloid leukemia. *Biomed Pharmacother.* 2023;168: 115820.
83. Venugopal S, Sekeres MA. Contemporary management of acute myeloid leukemia: a review. *JAMA Oncol.* 2024;10(10):1417–25.

Publisher's Note

Springer Nature remains neutral with regard to jurisdictional claims in published maps and institutional affiliations.